Calcium carbonate crystallization kinetics in the lime-soda ash water softening system

by

Larry Don Swinney

A Thesis Submitted to the
Graduate Faculty in Partial Fulfillment of the
Requirements for the Degree of
MASTER OF SCIENCE

Major: Chemical Engineering

Iowa State University
Ames, Iowa

1979

TABLE OF CONTENTS

NOMENCLATURE

a	Activity
A, B, α	Coefficients in Equation E.6
B^o	Nucleation rate, number/ml/minute
CO_3	Carbonate alkalinity, mg/l
d	Derivative operator
D_P	Particle diameter, cm
D_T	Total deposition of run, g
g	Gravitational acceleration, 32.2 ft/sec^2
G	Growth rate, microns/min
HCO_3	Bicarbonate alkalinity, mg/l
i	Kinetic order
I	Ionic strength, moles/liter
k_G	Rate constant in Equation E30
k_1, k_2, k_N	Coefficients in Equations E27, E28, E29
K	Equilibrium constant
K'	Corrected equilibrium constant
K_{sp}	Solubility product
L	Crystal length, microns
L_D	Dominant size, microns
m	Molality, kg solute/l suspension
M_T	Suspension density, g/l
n	Population density, numbers/ml/micron
n^o	Nuclei density, numbers/ml/micron

N	Cumulative number distribution
OH	Hydroxyl alkalinity, mg/l
pA	p operates on A and is equal to -log A
P	Phenolphthalein alkalinity, mg/l
Q	Flow rate, ml/min
S_a	Seed crystal surface area, cm^2
t	Time, min
t_T	Total time of run, min
T	Temperature, ^oK, in Equation (E 5) only
T	Total alkalinity, mg/l
V_T	Total volume of run
Z_j	Valence of j^{th} ion
[ ]	Concentration, moles/liter
γ	Activity coefficient
μ	Viscosity, g/cm sec
μ m	Micron
ρ	Density, g/ml
ρ_P	Particle density, g/ml
τ	Residence time, minutes

ABSTRACT

Although the lime-soda ash water softening process has been in use for over a hundred years, the precipitation kinetics of the softening reactions are not well understood. The kinetics of calcium carbonate precipitation have been studied in a continuous reactor operated under MSMPR conditions, first developed by Randolph and Larson for more concentrated crystallization systems. Reactor residence times, initial hardness levels, and effluent alkalinity distributions were varied to determine these kinetics. A Coulter Counter Model TA II was used to measure the crystal size distribution.

The kinetic data were fit with power-law models, indicating nucleation is a nonlinear function of crystal growth. Specifically, these models are:

$B^o = 1600\ G^{2.0}$ at T/P = 2.0, 225 ppm initial hardness

$B^o = 800\ G^{2.1}$ at T/P = 2.25, 225 ppm initial hardness

$B^o = 1.1 \times 10^5\ G^{5.2}$ at T/P = 1.4, 225 ppm initial hardness

$B^o = 7.3 \times 10^6\ G^{5.8}$ at T/P = 1.6, 350 ppm initial hardness

Residual hardness levels were lowest for the 350 ppm initial hardness runs. Crystal habit varies with effluent supersaturation, with aragonite crystals found at higher effluent supersaturations and calcite crystals formed at lower effluent supersaturations.

INTRODUCTION

The lime-soda ash water softening process has been used to remove hardness causing calcium and magnesium ions from municipal and industrial water supplies for over a hundred years (20, 38). Hard water is not considered detrimental to health, but calcium and magnesium ions increase soap consumption by forming insoluble precipitates with the soap. Hard water also often has unpleasant tastes and odors. Calcium carbonate and magnesium-silicate scales deposit in industrial heat exchangers, lowering heat transfer coefficients, while calcium carbonate scale forms in municipal pipes and consumer bath tubs and water heaters.

In the past, the reactions in the lime-soda ash water softening process have been assumed to equilibrate in the reactor. However, these equilibrium reactions do not describe the precipitation kinetics of the reactions in continuous processes. These kinetics are not well understood. Presently, softening plant design methods use empirically set amounts of excess lime treatment. A clear understanding of the precipitation kinetics would allow optimum plant design to provide adequate softening yet relatively large particles to facilitate solid-fluid separation. The determination of the nucleation and growth kinetics to obtain more reliable design information is the primary goal of this research. Specifically, the kinetics of calcium carbonate precipitation have been studied.

Crystallization is one of the oldest unit operations, but

knowledge concerning crystallization kinetics has been obtained only in the last 20 years. Randolph and Larson (33) applied the population balance to model various modes of crystallizer operation assuming the crystal size distribution (CSD) is known. Several authors (1, 8, 19, 22, 31, 37, 39) have employed the Randolph-Larson model to crystallization systems with high solute concentrations.

Schierholz (37) studied the kinetics of calcium carbonate precipitation from reaction of calcium sulfate and sodium carbonate and found the Randolph-Larson model can also be applied to dilute systems. In the present study, calcium carbonate was precipitated from calcium bicarbonate reaction with lime. During the course of his experiments, Schierholz scraped his reactor to prevent crystal buildup on reactor surfaces. This scraping may have violated a number of the Randolph-Larson model assumptions. The objective of this project is to determine precipitation kinetics without reactor scraping and with calcium bicarbonate as the hardness-imparting compound.

Reactor effluent alkalinity distributions, initial calcium bicarbonate levels, and reactor residence time were varied to determine the precipitation kinetics. All experiments were performed in a continuous, well-mixed reactor operated under Randolph-Larson model conditions. A Coulter Counter Model TA II was utilized to measure the crystal size distribution in the experiments.

The kinetic data obtained in this study fit the Randolph-Larson

model well for each set of reactor conditions, but the kinetic order of nucleation varies as reactor conditions changed. Residual hardness levels were lowest in runs where the initial hardness levels were the highest. Crystal habit varies with effluent supersaturation. Dendritic aragonite crystals form when effluent supersaturations are high, and rhombic calcite crystals are produced at lower effluent supersaturations.

LITERATURE REVIEW AND BACKGROUND

The literature review for this research must cover a variety of topics. These topics include municipal lime-soda ash water softening processes, water chemistry, reactions and equilibria, and reactor pH and alkalinity effects in the softening process. The population model is employed to develop kinetic models which yield fundamental equations needed for crystallizer design. Several previous studies provide useful information concerning calcium carbonate crystallization kinetics.

Lime-soda Ash Water Softening Reactions

Municipalities have used lime and soda ash to soften water before distribution to their customers for over a hundred years (20, 38). Hard water is defined as containing objectionable amounts of dissolved calcium and/or magnesium salts. These salts are removed in the softening process so that only 80-120 mg/l (as $CaCO_3$) hardness remains.

There are two types of water hardness, carbonate and noncarbonate. Carbonate hardness consists of calcium and magnesium bicarbonates [$Ca(HCO_3)_2$ and $Mg(HCO_3)_2$] and is also known as temporary hardness because, as water containing carbonate hardness is boiled, CO_2 gas is expelled, and less soluble carbonates are formed. Noncarbonate hardness includes sulfates and chlorides of calcium and magnesium ($CaSO_4$, $CaCl_2$, $MgSO_4$, $MgCl_2$) and is impervious to boiling. For this reason, noncarbonate hardness is also called permanent

hardness.

Municipally, bicarbonates are not removed by boiling, but by adding calcium hydroxide (lime) to the hard water in a stirred tank reactor. The lime forms precipitates of calcium carbonate and magnesium hydroxide:

$$Ca(HCO_3)_2 + Ca(OH)_2 \rightleftarrows 2CaCO_3 \downarrow + 2H_2O \quad (R1)$$

$$Mg(HCO_3)_2 + Ca(OH)_2 \rightleftarrows MgCO_3 + CaCO_3 \downarrow + 2H_2O \quad (R2)$$

$$MgCO_3 + Ca(OH)_2 \rightleftarrows CaCO_3 \downarrow + Mg(OH)_2 \downarrow \quad (R3)$$

Lime and sodium carbonate (soda ash) are both needed to chemically precipitate noncarbonate hardness. Again, calcium carbonate and magnesium hydroxide are formed:

$$MgCl_2 + Ca(OH)_2 \rightleftarrows Mg(OH)_2 \downarrow + CaCl_2 \quad (R4)$$

$$CaCl_2 + Na_2CO_3 \rightleftarrows CaCO_3 \downarrow + 2NaCl \quad (R5)$$

$$CaSO_4 + Na_2CO_3 \rightleftarrows CaCO_3 \downarrow + Na_2SO_4 \quad (R6)$$

$$MgSO_4 + Na_2CO_3 + Ca(OH)_2 \rightleftarrows Mg(OH)_2 \downarrow + CaCO_3 \downarrow + Na_2SO_4 \quad (R7)$$

In addition, there are numerous side reactions and equilibria:

$$CO_2 + Ca(OH)_2 \rightleftarrows CaCO_3 \downarrow + H_2O \quad (R8)$$

$$Ca(HCO_3)_2 \rightleftarrows CaCO_3 \downarrow + CO_2 + H_2O \quad (R9)$$

$$H_2CO_3 \rightleftarrows H^+ + HCO_3^- \quad (R10)$$

$$HCO_3^- \rightleftarrows H^+ + CO_3^= \quad (R11)$$

$$H_2O \rightleftarrows H^+ + OH^- \quad (R12)$$

Workers in the water softening industry generally express hardness and alkalinity concentrations in terms of milligrams per liter (mg/l) or parts per million (ppm) as calcium carbonate. Water with a given ppm hardness has the same number of calcium and magnesium equivalents as water containing the same ppm calcium carbonate. Other ions are expressed as $CaCO_3$ by multiplying the number of equivalents of these ions by a conversion factor. Since calcium carbonate is a bivalent compound with a molecular weight of 100, this conversion factor is 50,000 mg $CaCO_3$ per equivalent.

Municipal Water Softening Processes

The lime-soda ash water softening process has undergone several refinements in the last several years. These include excess lime treatment, split treatment, and sludge recycle.

The equilibrium relations show that stoiciometric amounts of lime are sufficient to soften calcium bicarbonate, but excess lime is needed to remove magnesium bicarbonate. Figure 1 depicts a typical two-stage excess lime softening plant. Raw water is aerated to remove dissolved gases and to convert soluble ferrous iron ions to insoluble ferric ions. The water is mixed with excess lime in the first of a series of three tanks. Most carbonate hardness is precipitated in this reactor. The second tank, needed for flocculation and agglomeration of the precipitates, is slowly mixed. The third tank is quiescent and is used to allow the solids to settle out of

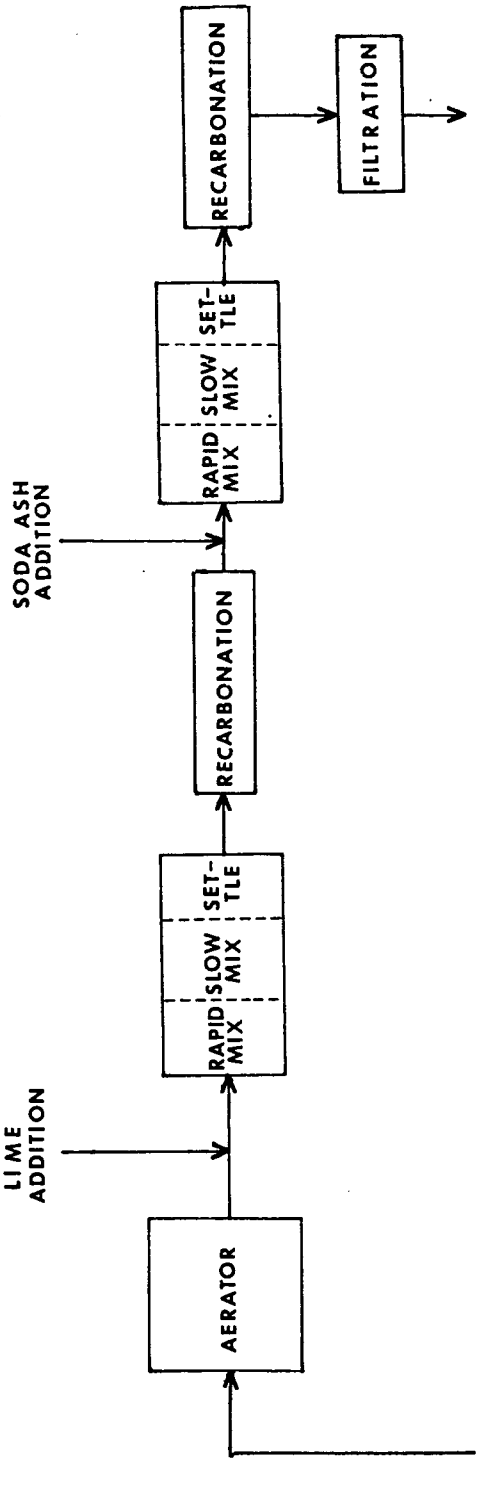

Figure 1. Flow diagram for a typical two-stage lime-soda ash water softening plant

the treated water. From this tank series, the water is recarbonated to lower the pH and sent to the first of another set of three tanks. Soda ash treatment takes place in this tank series. After this second tank battery the water is again stabilized by recarbonation, filtered to remove unsettled particles, and distributed to customers.

Split treatment is employed by many municipal softening plants. In this scheme, most of the raw water is treated with excess lime. The untreated fraction of the water neutralizes this excess lime in a subsequent step. The Ames softening plant uses this method, as shown in Figure 2. After the initial aeration step, 20-25 percent of the raw water is split from the water and sent directly to the second reactor. Excess lime is rapidly mixed with the rest of the raw water in the first reactor for a few minutes. This water is then mixed with the untreated water, recycled sludge (a combination of previously precipitated calcium carbonate and magnesium hydroxide), and, occasionally, soda ash in the second reactor. This reactor is slowly mixed for 20-30 minutes. The high cost of soda ash and the relatively low noncarbonate hardness levels in Ames groundwater necessitate the infrequent use of soda ash (Harris Seidel, Ames, Iowa Water Treatment Plant, 1978, private communication). The treated water is stored in a quiet settling tank for two to three hours to allow solids to settle out of the suspension. Polyphosphates are added before filtration to prevent calcium carbonate and iron precipitation on the sand filters. Less recarbonation is required for split treatment than for excess

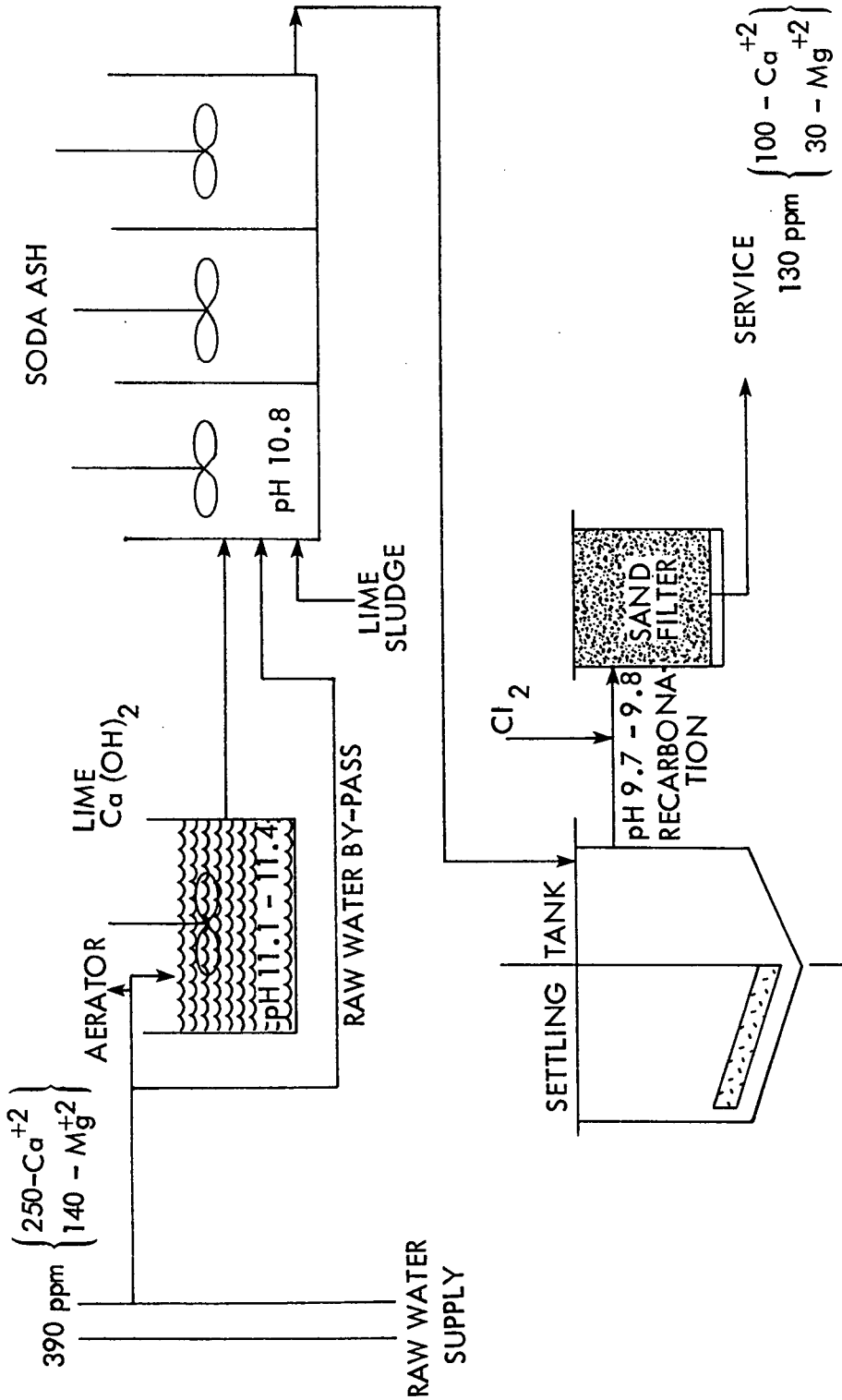

Figure 2. Ames water treatment plant

lime treatment due to dissolved carbon dioxide and bicarbonates (12). After filtration, the water is distributed to Ames customers.

The heart of the water softening process, the reaction of raw water with lime and soda ash, is essentially a reactive crystallization process. Sawyer and McCarty (36) noted the minimum residual calcium carbonate and magnesium hydroxide levels in the softening process are 17 mg/l and 9 mg/l, respectively. Larson, Lane, and Neff (24) reported these conditions are rarely reached during the softening reactions. Behrman and Green (4) noted that, in actual practice, residual hardness levels of 50-60 mg/l are obtained, roughly 2-3 times the minimum levels. A number of authors (4, 36) believed that this increase is due to a supersaturated solution of calcium carbonate and magnesium hydroxide formed during softening which hinders the precipitation. Larson, Sollo, and McGurk (25) theorized that this supersaturation is due to the formation of stable, soluble complexes. These proposed complexes are comprised of calcium, magnesium, and sodium cations with sulfate, carbonate, bicarbonate, and hydroxide anions. The most important complexes are $CaCO_3$, $MgCO_3$, and $CaSO_4$ (25). Larson et al. (25) defined dissociation constants for several complexes and determined their values at 5, 15 and 25°C. For example, the dissociation constant for calcium carbonate,

$$K_{dCaCO_3} = a_{Ca^{++}} a_{CO_3^{=}} / a_{CaCO_3} \qquad \text{(E1)}$$

was found to equal 5.98×10^{-4} at 25°C. As expected from Equation (E1) the complexes of $CaCO_3$, $CaSO_4$, and $MgCO_3$ had the smallest values, corresponding to the largest complex activities at given ionic activities.

Mullin (27) proposed a general crystallization theory consistent with these observations. Figure 3 shows three distinct zones in the solubility-temperature curve for a typical compound: a labile region where spontaneous nucleation takes place; an unsaturated region where nucleation cannot occur; and a metastable region where spontaneous nucleation is rare but addition of crystal seeds generated much nucleation. This metastable region corresponds to the stable supersaturated region proposed for the softening reactions.

In many softening plants, a portion of the precipitated sludge from the settling tank is pumped back into the reactor. This sludge enhances the reaction in terms of completeness and speed (4). This seeding increases the surface area available in the reactor to relieve supersaturation. The addition of sludge recycle at the Ames treatment plant enabled doubling the plant capacity at a cost of one-fifth that of other methods of doubling capacity (6).

The treated water leaving the settling tanks is quite basic. If left in this state, the water will deposit calcium carbonate scale on the sand filters and in the distribution lines. While a small amount of scale is beneficial to protect distribution lines, the lines will eventually become plugged unless the pH is lowered.

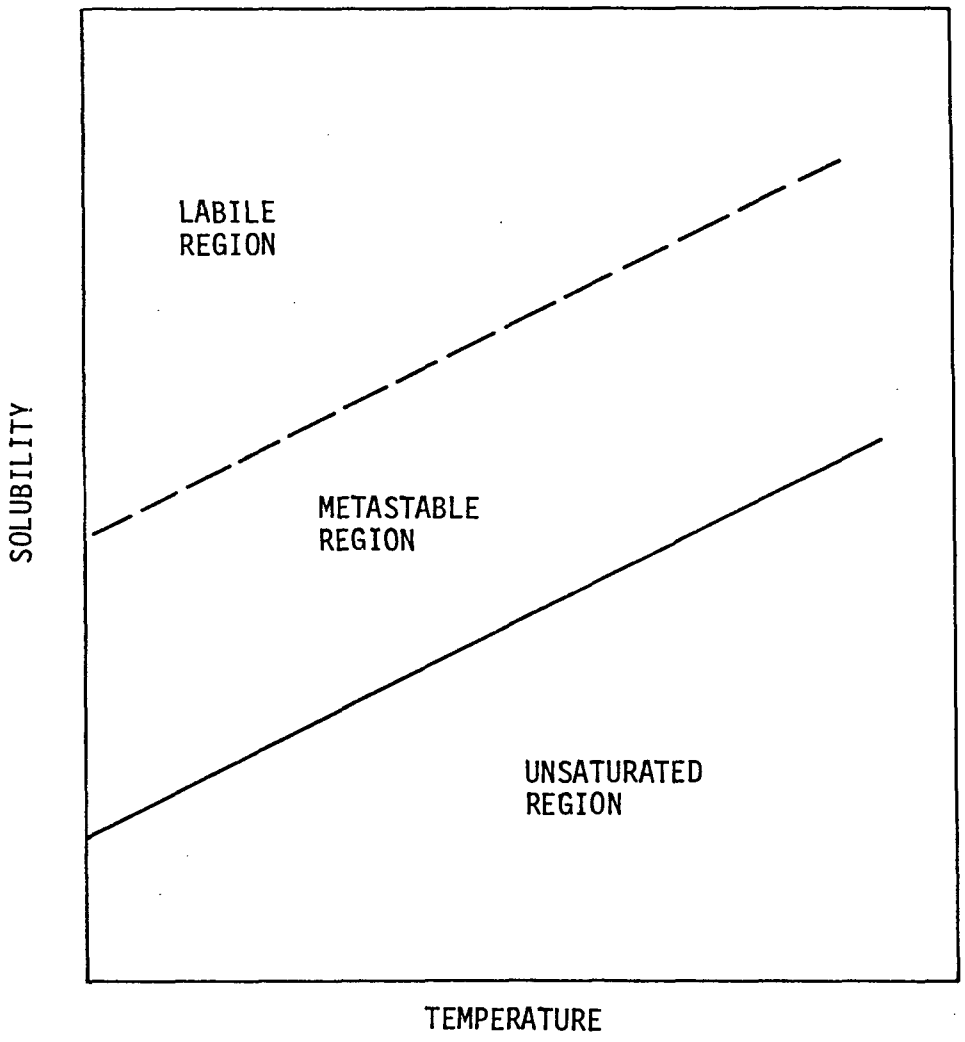

Fig. 3. Region of stable supersaturation

One way to accomplish this is by recarbonation:

$$Ca(OH)_2 + CO_2 \rightleftarrows CaCO_3 \downarrow + H_2O \qquad (R13)$$

Langelier (21) developed a Saturation Index to quantify this scaling tendency:

$$S.I. = \text{Saturation Index} = pH_{actual} - pH_{saturation} \qquad (E2)$$

where $pH_{saturation}$ is a function of equilibrium constants, calcium concentration, and alkalinity. A positive Saturation Index indicates scale deposition, a negative S.I. predicts scale dissolution, and a Saturation Index of zero means that the water is in equilibrium with the scale. However, Feitler (15) noted a pH of 0.6-1.0 units above the calculated saturation pH is necessary for a stable water.

Ryznar (35) developed a similar index to predict scale formation, the Stability Index:

$$\text{Stability Index} = 2pH_{saturation} - pH \qquad (E3)$$

A Stability Index of six or less indicates scale forming, while values of seven or more predict scale dissolution.

Solubility and Dissociation

Several factors combine to complicate the precipitation of calcium carbonate. The solubility product, which defines the theoretical minimum calcium carbonate level in equilibrium with precipitated calcium carbonate, is dependent on water temperature and ionic strength. Since calcium carbonate is the salt of a weak acid, the carbonate ions equilibrate with the acid and the

intermediate bicarbonate ions, thus reducing the total number of carbonate ions available for precipitation. The dissociation of calcium carbonate and the ionization of water are coupled with this equilibrium, also influencing precipitation.

Calcium carbonate solubility

The theoretical solubility of calcium carbonate at a given temperature and ionic strength is found by first determining the solubility product, K_{sp}, at a given temperature and then adjusting the K_{sp} to account for the ionic strength of the solution.

Calcium carbonate dissolution is given by the equilibrium relation:

$$CaCO_3(s) \rightleftarrows Ca^{++}(1) + CO_3^{=}\ (1) \qquad \text{(R14)}$$

The solubility product is represented by:

$$K_{sp} = a_{Ca^{++}}\, a_{CO_3^{=}} = [Ca^{++}][CO_3^{=}]\ \gamma_{Ca^{++}}\gamma_{CO_3^{=}} = K_{sp}'\ \gamma_{\pm}^2 \qquad \text{(E4)}$$

where: K_{sp} is the solubility product; K_{sp}' is the corrected solubility product, $[Ca^{++}][CO_3^{=}]$; and $\gamma_{\pm}^2$ is the product of the calcium and carbonate activity coefficients.

At 25°C, K_{sp} for calcium carbonate ranges from (4 to 5) x 10^{-9} (23, 25, 42). Calcium carbonate is somewhat unusual among acid salts in that its solubility decreases as temperature increases. Several sources (14, 23, 32) present K_{sp} values as a function of temperature. Schierholz (37) developed the following equation to describe these data:

$$\log K_{sp} = -8.021586 + 488.89891/T - 0.00655641T \qquad (E5)$$

where T is in Kelvin degrees.

The dependence of the solubility product on ionic strength is described in many physical chemistry books, including Adamson (2). In systems where very small concentrations of calcium and carbonate ions are present, the activity coefficient $\gamma_{\pm}$ approaches unity. As the ionic concentrations increase, however, interionic interactions become important. The activity coefficients decrease, and the corrected solubility must increase to retain the equality in Equation (E4). In water softening, the ionic concentrations are sufficiently dilute to warrant use of Debye-Huckel theory to predict activity coefficients for the various ions.

$$\log \gamma_j = \frac{-Az_j^2 \sqrt{I}}{1 + \alpha B \sqrt{I}} \qquad (E6)$$

where: z_j = valence of ion j

I = ionic strength

A, B, α = coefficients

Garrels and Christ (16) give values for these constants which show A and B are slightly dependent on temperature, while α is a function of ionic strength. Larson and Buswell (23) fit experimental solubility-ionic strength data with this equation:

$$pK_{sp}' = pK_{sp} - 4\sqrt{I} \,/\, (1 + 3.9\sqrt{I}) \qquad (E7)$$

This equation is derived by combining Equations (E4) and (E5).

The ionic strength of a solution can be determined a number of ways. One (2) is given by:

$$I = \tfrac{1}{2} \sum_j m_j \, z_j^2 \qquad \text{(E8)}$$

where m_j is the molality of the ion j. In this work, ions in solution include OH^-, $CO_3^=$, HCO_3^-, Cl^-, Ca^{++}, Na^+, and H^+. Langelier (21) presented a simpler expression,

$$I = 0.000025 \times (\text{total mineral content}) \qquad \text{(E8a)}$$

which is valid for mineral content less than 500 ppm. The total mineral content is found by evaporating a weighed sample of water, weighing the remaining solids and dividing this weight by the original sample weight. The ionic strength can also be determined from conductivity measurements. The conductivity meter must be calibrated with solutions of known molalities to determine the ionic strength at a particular conductivity.

These equations can be used to determine calcium carbonate solubility when the temperature and ionic strength are known.

Dissociation of carbonic acid and water

The dissociation of water and carbonic acid are treated in much the same way as for calcium carbonate. Corrected dissociation constants are defined in terms of concentration and ionic strengths (12, 23).

The dissociation of carbonic acid is described by the following

equilibria:

$$H_2CO_3 \rightleftarrows H^+ + HCO_3 \qquad \text{(R10)}$$

$$HCO_3^- \rightleftarrows H^+ + CO_3^= \qquad \text{(R11)}$$

At the basic conditions encountered in water softening, the first reaction goes to completion. The second dissociation constant, K_2, is defined by

$$K_2 = \frac{a_{CO_3^=}\, a_{H^+}}{a_{HCO_3^-}} = K_2' \gamma_{CO_3^=} \gamma_{H^+} / \gamma_{HCO_3^-} \qquad \text{(E9)}$$

where $K_2' = [CO_3^=][H^+] / [HCO_3^-]$. Similarly, dissociation constant for water is

$$K_w = K_w' \gamma_{OH^-} \gamma_{H^+} / \gamma_{H_2O} \qquad \text{(E10)}$$

where $K_w' = [H^+][OH^-] / [H_2O]$.

Harned and Owen (17) and Harned and Scholes (18) listed K_w and K_2 as functions of temperature. Larson and Buswell (23) defined the following corrected dissociation constants as functions of ionic strength:

$$pK_w' = pK_w - \sqrt{I} \,/\, (1 + 1.4\sqrt{I}) \qquad \text{(E11)}$$

$$pK_2' = pK_2 - 2\sqrt{I} \,/\, (1 + 1.4\sqrt{I}) \qquad \text{(E12)}$$

Alkalinity

The alkalinity of a natural water is defined as its ability to neutralize acids. For many years, the primary parameter in water softening plant operation was the pH level in the reactor, with little consideration given to alkalinity. This has changed in the last several years (37), because the alkalinity distribution influences both calcium carbonate solubility and precipitation kinetics (31, 37).

Alkalinity is imparted to a water by the carbonate, bicarbonate, and hydroxyl ions. Borates, silicates, and phosphates, if present, also contribute to the alkalinity (36), but usually only an insignificant amount. Alkalinity is measured by titration of a known volume with a strong mineral acid of known normality to two indicator endpoints. The first indicator, phenolphthalein, turns colorless at pH = 8.3, the bicarbonate equivalence pH. This represents the phenophthalein alkalinity. The second indicator changes color at a pH of 4.5-5.0, the carbonic acid equivalence point, denoting the total alkalinity.

The total alkalinity, T, is defined as the total concentration of all cations in solution associated with the hydroxyl, carbonate, and bicarbonate ions except the hydrogen ion. In terms of mg/l as calcium carbonate, T is expressed in equation form as

$$H + T = CO_3 + HCO_3 + OH \qquad \text{(E13)}$$

where CO_3 represents the carbonate alkalinity, etc. In

terms of concentrations, this equation is

$$[H^+] + T/50{,}000 = [HCO_3^-] + 2[CO_3^=] + [OH^-] \quad \text{(E14)}$$

50,000 is the conversion factor from mg/l as $CaCO_3$ to equivalents/liter, and there are two equivalents per mole of carbonate ion. For systems with pH greater than 9.5, the hydrogen alkalinity and concentration can be ignored (36).

The phenolphthalein alkalinity, P, represents the amount of acid needed to neutralize essentially all the hydroxyl ions and convert the carbonate ions to bicarbonate ions. In equation form this becomes

$$P = CO_3/2 + OH \quad \text{(E15)}$$

in mg/l as $CaCO_3$ units and

$$P/50{,}000 = [CO_3^=] + [OH^-] \quad \text{(E16)}$$

in terms of concentrations.

A number of ways exist to calculate carbonate, bicarbonate, and hydroxyl alkalinities in a water of known total and phenolphthalein alkalinities. Standard Methods (40) presented relationships between the three anionic concentrations as a function of the ratio of phenolphthalein alkalinity to total alkalinity. These values are qualitative at best because the relationships assume neither carbon dioxide and carbonate nor hydroxyl and bicarbonate can coexist in a water. A number of authors (5, 36) presented plots which indicate this assumption is inaccurate. Sawyer and McCarty (36)

noted Equations (E14) and (E16) can be easily solved for carbonate and bicarbonate concentrations, given the total and phenolphthalein alkalinities and the pH of the water.

A substantially more complicated method to determine carbonate and bicarbonate alkalinities utilizes equilibrium relationships discussed in the previous section (5, 12, 37). Equations (E14) and (E16) are combined to obtain

$$[HCO_3^-] = \frac{T/50{,}000 + [H^+] - K_w'/[H^+]}{1 + 2K_2'/[H^+]} \qquad \text{(E17)}$$

and

$$[CO_3^=] = \frac{T/50{,}000 + [H^+] - K_w'/[H^+]}{2(1 + [H^+]/2K_2')} \qquad \text{(E18)}$$

Providing all equilibria have been reached, the proper constants for K_2' and K_w' can be incorporated into Equations (E17) and (E18) to calculate the bicarbonate and carbonate concentrations if the water pH, temperature, and ionic strength are known. Since these calculations are quite involved, the method using Equations (E14) and (E16) with a knowledge of water pH, total and phenolphthalein alkalinities to calculate carbonate and bicarbonate concentrations is easier to implement.

The Population Balance

For many processes analyzed by chemical engineers, heat and mass balances, along with rate equations, can be judiciously applied to quantify the system. In the lime-soda ash water softening process where solid particles nucleate and grow, however, these balances tell us the mass of crystals produced but not the size and number of crystals. Randolph and Larson (33) developed a population balance to describe the crystal size distribution (CSD) of particulate systems.

The population balance contends the number of discrete particles must be conserved in a dispersed system. All particles can be accounted for by crystal birth and death rates, flow rates, and a knowledge of the CSD at any particular moment in the crystallizing vessel. The performance of many industrial crystallizers, including the reactors used in unseeded water softening processes, can be represented by the continuous mixed-suspension, mixed-product-removal (MSMPR) crystallizer model. The MSMPR model can be altered to describe variations in MSMPR operation such as seeded water softening reactors. Randolph and Larson (33) presented detailed derivations of the MSMPR model and variations.

An important quantity in the population balance is the population density, defined as the number of particles per unit volume per particle size range, or, in differential form:

$$n = \lim_{\Delta L \to 0} \frac{\Delta n}{\Delta L} = \frac{dN}{dL} \tag{E19}$$

where n = population density

N = numbers/unit volume

L = length

The population density n depends on the crystal size at which the interval ΔL was taken.

Mixed-suspension, mixed-product-removal (MSMPR) model

The continuous mixed-suspension, mixed-product-removal (MSMPR) has been applied to various crystallization systems by several authors (8, 19, 31, 37, 39, 41). The MSMPR model utilizes several assumptions which greatly simplify the mathematical analysis while adequately describing crystallizer operation. These assumptions are:

(1) Crystallizer is well mixed

(2) Crystallizer operates under steady-state conditions

(3) No crystals in feed streams

(4) Negligible crystal breakage and attrition

(5) Unclassified product removal from crystallizer

(6) Crystal growth is not a function of length

Figure 4 depicts a constant volume, continuous MSMPR crystallizer. The above assumptions are incorporated into a population balance around a size range ΔL and a time period Δt to obtain

$$n = n^{o}\exp(-L/G\tau) \qquad \text{(E20)}$$

where: n^{o} = nuclei density, numbers/μm ml

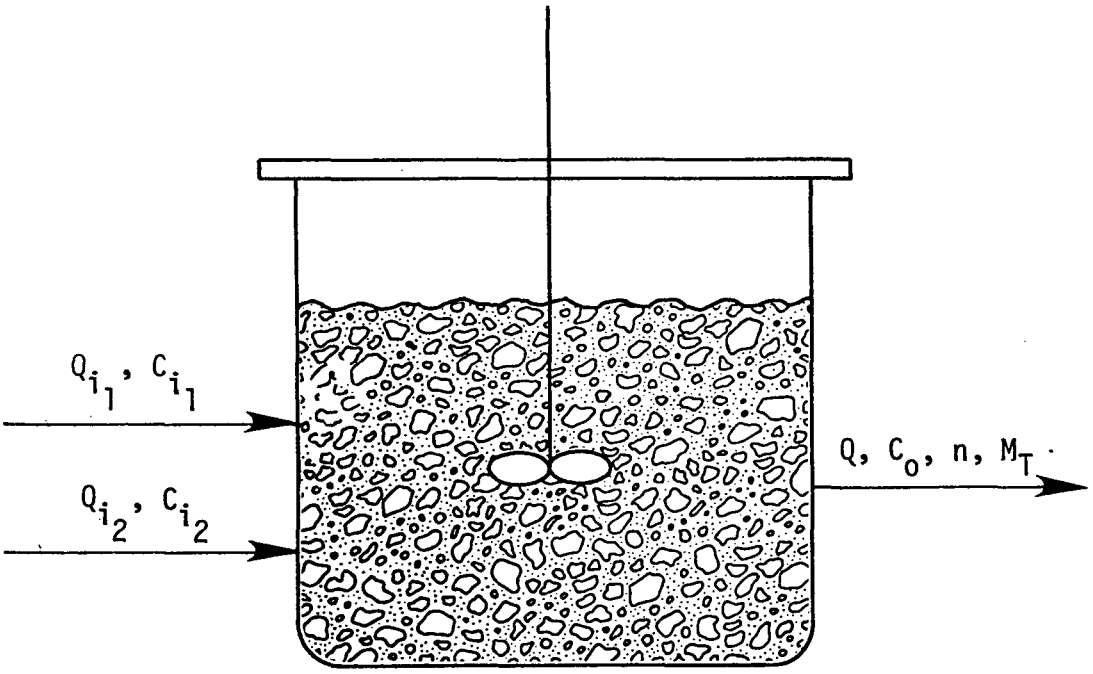

Figure 4. Schematic diagram for crystallizer

G = growth rate, μ m/ min

τ = mean residence time, min

Substituting this expression for the population density into the integral form of Equation (E19) and integrating from size L to ∞ yields (9):

$$N(L,\infty) = n^{o}G\tau \exp(-L/G\tau) \tag{E21}$$

Therefore, a plot of ln N versus L has a slope $-1/G\tau$ and an intercept of $n^{o}G\tau$.

The nucleation rate B^{o}, the rate of formation of stable nuclei, can be represented as the product of two differentials:

$$B^{o} = (dN/dt)_{L\rightarrow 0} = (dN/dL)_{L\rightarrow 0}\ (dL/dt) \tag{E22}$$

The second differential represents the growth rate G. From Equation (E19), the first differential is the definition of the nuclei density. So,

$$B^{o} = n^{o}G \tag{E23}$$

Hence, solution of Equation (E21) yields both the nucleation and growth rates in the MSMPR crystallizer.

The population density equation for the MSMPR model, Equation (E19), can be combined with the integral form of the definition of population density to obtain

$$N = \int_{0}^{L} n^{o}\exp(-L/G\tau)dL \tag{E24}$$

This equation, which gives the total number of crystals up to size L, is called the zeroth moment of the number distribution. The integrand is multiplied by L^m, where m equals one, two, or three, to obtain the first, second, and third moments, respectively. The total mass of the crystals equals the third moment multiplied by a volume shape factor, k_v, and the crystal density, ρ:

$$M_T = k_v \rho \int_0^L n^o L^3 \exp(-L/G\tau)\, dL \qquad \text{(E25)}$$

As L becomes large, this integrates to

$$M_T = 6 \rho k_v n^o (G\tau)^4 \qquad \text{(E26)}$$

Nucleation is a complex process involving the coming together of a critical number of molecules which pass over an energy barrier to form a stable nucleus. Several theoretical nucleation models have been proposed (27), but none have proven satisfactory for all crystallization systems. Randolph and Larson (33) have reported considerable success in several systems with an empirical power-law model

$$B^o = k_1 (c-c_s)^i = k_1 s^i \qquad \text{(E27)}$$

where: s = supersaturation

k_1 = kinetic constant

i = kinetic order of nucleation

The growth rate is generally considered a linear function of supersaturation,

$$G = k_2 s \tag{E28}$$

where k_2 is another constant. These expressions can be combined to eliminate the supersaturation s yielding

$$B^o = k_N G^i \tag{E29}$$

The parameters i and k are found by performing a set of experiments in which residence time is changed to vary the supersaturation and plotting ln B^o vs ln G for these experiments. Since the total mass of crystals must be conserved, Equation (E26) tells us that, as the residence time decreases, the growth rate (and the supersaturation) must increase.

Calcium Carbonate Crystallization Kinetic Studies

For many years, research in the water softening field stressed the equilibrium relationships involved. In the last ten years, however, several studies have been reported which deal with the kinetics of the softening reactions. These studies have been conducted in both batch and continuous systems.

The batch system studies have emphasized the change in calcium concentration with respect to time, or $d[Ca^{++}]/dt$. Reddy and Nancollas (28, 34) initiated nucleation by adding calcite seed crystals to supersaturated calcium carbonate solutions with 14-44 ppm (as $CaCO_3$) initial calcium and 18-38 ppm (as $CaCO_3$) initial carbonate concentrations. The calcium and carbonate concentrations were observed to fit the following equation:

$$d[Ca^{++}]/dt = -k_G S_a \left([Ca^{++}][CO_3^{=}] - K_{sp}/\gamma_{\pm}^2\right) \quad \text{(E30)}$$

where k_G is a rate constant and S_a is the seed crystal surface area. They also found the calcite crystal growth was a linear function of the weight of seed crystal used. Wiechers, et al. (43) also used calcite seed crystals, but with initial calcium concentrations of 70-300 ppm as $CaCO_3$. Measuring only pH as a function of time and calculating calcium and carbonate assuming equilibria had been achieved, they verified Equation (E30). Alexander and McClanahan (3) initiated nucleation by mixing solutions of calcium ions and bicarbonate ions as opposed to seeding. They determined apparent equilibria had been reached after 25 minutes. The equilibria were dependent on initial pH values, but independent of initial calcium concentration (3). $[Ca^{++}]_{initial}/[Ca^{++}]$ vs. time plots indicated first order precipitation kinetics with respect to calcium ion concentration.

Since the lime-soda water softening reactors operate continuously, the above batch studies are not representative of this process. For example, Wiechers et al. (43) noted markedly different rate vs. pH data for $CaCO_3$ seed crystals manufactured by different companies, indicating that recycled sludge from a softening plant should be used as seed crystals for accurate batch data. To prevent this complication, kinetic studies in continuous crystallizers have been performed. These studies require population balance data as well as concentration vs. time data. Maruscak et al. (26)

used the Randolph-Larson MSMPR model to model growth kinetics. However, their reactant concentrations were sufficiently high to induce agglomeration, which prevented the use of a linear growth model.

Schierholz (37) was the first to perform a continuous calcium carbonate reactor study using initial hardness levels similar to those found in actual practice. He studied the removal of non-carbonate hardness:

$$CaSO_4 + Na_2CO_3 \rightleftarrows CaCO_3 \downarrow + Na_2SO_4 \qquad (R6)$$

Using an initial feed tank hardness of 442 ppm as $CaCO_3$, he used reactor residence times of 10, 20, and 30 minutes for three alkalinity distributions. The growth-nucleation data obtained fit the power law kinetic model as follows:

$$B^o = 57{,}000\ G^2$$

$$B^o = 28{,}000\ G^{1.7}$$

$$B^o = 37{,}000\ G^{1.7}$$

at T/P alkalinity ratios of 3.3, 4.3, and 2.1, respectively. Softening efficiencies ranged between 87 and 94%.

Schierholz verified the feasibility of applying Randolph-Larson MSMPR model to low suspension density systems, but his experimental procedure did not closely approximate actual practice in two ways. First, the reaction system is not representative of actual systems because lime is not used as a softening agent.

Hence, his initial calcium levels are low because lime adds calcium hardness to the water. Secondly, he minimized calcium carbonate wall scale during the reaction by scraping the walls to return the scale to the suspension. This scraping violated the MSMPR assumption of no crystals in the feed streams, as the scraped scale added many sites for crystal nucleation. In addition, the scraping caused crystal breakage, thus violating another MSMPR assumption. A better experimental technique would be to allow the wall scale to build up throughout the experiment. This would prevent a true steady state from being reached; however, the total wall accumulation could be easily determined at the end of the experiment.

Peters (31) studied calcium carbonate and magnesium hydroxide coprecipitation in a continuous reactor without wall scraping. He reacted calcium bicarbonate and magnesium sulfate with sodium hydroxide to form calcium carbonate and magnesium hydroxide. Like Schierholz, Peters varied reactor residence time and alkalinity distribution to obtain

$$B^o = 75{,}600\ G^{3.2}$$

and

$$B^o = 31{,}200\ G^{2.4}$$

at T/P = 1.75 and 2.0, respectively. Calcium softening efficiencies ranged from 76 to 91%.

Although two components were precipitated, Peters treated the system as a pseudo-one component system. Since the magnesium

hydroxide crystals were smaller than the calcium carbonate crystals, the MSMPR model indicates this combination of the components yielded a smaller calculated growth rate and larger nucleation rate than if the magnesium were not present.

Dabir (8) performed a study similar to those of Schierholz and Peters except he studied the reaction of magnesium chloride and sodium hydroxide to form magnesium hydroxide. He varied residence time at conditions of 20% excess, stoiciometric, and 20% deficient NaOH. The nucleation-growth equations found were:

$$B^o = 1.7 \times 10^7 \, G^{2.7}$$

$$B^o = 3.6 \times 10^4 \, G^{1.6}$$

$$B^o = 1.4 \times 10^3 \, G^{1.0}$$

at 20% excess, stoiciometric, and 20% deficient NaOH, respectively. This research is significant because a linear relationship was found between the kinetic order i and the hydroxide concentration in the reactor (41).

THE OBJECTIVE

The objective of this research is determining the kinetics of calcium carbonate precipitation in a continuous lime water softening reactor.

In many chemically reacting systems, rate equations, heat and mass balances can quantitatively describe the system. In the water softening process, however, a population balance is needed to describe the nucleation and growth of crystals formed during the reaction. The population balance is simplified through several assumptions to form the mixed-suspension, mixed-product-removal (MSMPR) crystallizer model. Since unseeded municipal softening reactors approximate MSMPR operation, an MSMPR crystallizer was used in this study.

Water softening is different from most crystallization processes in two major aspects. First, the suspension densities involved are much less than in most industrial crystallization processes. Crystals in more concentrated systems usually grow large enough to perform sieve analyses to determine the crystal size distribution (CSD). For the more dilute water softening process, however, the crystals are too small for sieves, and another sizing device is necessary. The Coulter Counter Model TAII was used to determine the CSD in this study. Secondly, the mother liquor in most crystallizations is a byproduct, whereas in water treatment the mother liquor (water) is the desired product and the crystals

are byproducts. Therefore, this study requires careful understanding and monitoring of the water chemistry as well as the crystallization kinetics of the process.

Schierholz (37) studied $CaCO_3$ crystallization kinetics in a calcium sulfate-sodium carbonate system using continuous reactor conditions approximating actual practice. Several questions have arisen since his study. First, Schierholz scraped crystal buildup from the reactor walls, a procedure since believed to have violated several MSMPR assumptions. He found both the kinetic order i and the nucleation-growth equation constant k_N were largest at stoiciometric chemical additions, while researchers studying similar systems (8, 31, 41) found both i and k_N increased with treatment chemical dosage when the reactor was not scraped. Dabir (8) and Stevens et al. (41) found the kinetic order increased linearly with hydroxyl dosage in a system utilizing sodium hydroxide to precipitate magnesium hydroxide. Will i and k_N also increase as lime dosage increases in calcium carbonate precipitation when the reactor is not scraped? If so, is the kinetic order linear with respect to a particular ionic concentration or a product of ionic concentrations? Second, since lime is used to soften water more frequently than sodium carbonate, how does lime usage affect the kinetics? Third, how do initial hardness level variations affect the kinetics?

These questions were addressed by studying the reaction of calcium bicarbonate with calcium hydroxide in a continuous reactor under carefully controlled conditions. The reactor residence times,

hydroxyl ion dosages, and initial hardness levels were varied to determine the crystallization kinetics.

EXPERIMENTAL

Experimental Equipment

Figure 5 is a flow diagram of the experimental apparatus. Figures 6 and 7 are pictures of the equipment. The equipment is similar to that used by Peters (31) except that a time delay for reactor withdrawal was not used, new flowmeters were installed, and floats were used to reduce CO_2 absorption in the feed tanks.

Crystallizer

The crystallizer was a 20-liter capacity plexiglass vessel. The crystallizer and accompanying plexiglass cover are diagrammed in Figure 8. It was designed to minimize the wall surface area to volume ratio as described by Peters (31). All experimental runs were conducted with a reactor volume of 16 liters.

The crystallizer contents were stirred with a 14-inch glass impeller with four pitched blades. The ratio of blade diameter to reactor diameter was 0.24, and the pitch of the blades was 1.0. Early runs indicated an agitation speed of 525 revolutions per minute prevented particle settling in the crystallizer. A Cole-Parmer control unit (Model 600-013, 0-1000 rpm) and driver powered the impeller.

Coulter counter

A Coulter Counter Model TAII with population accessory was employed to determine the crystal size distribution.

In the Coulter Counter, a vacuum system is used to draw an

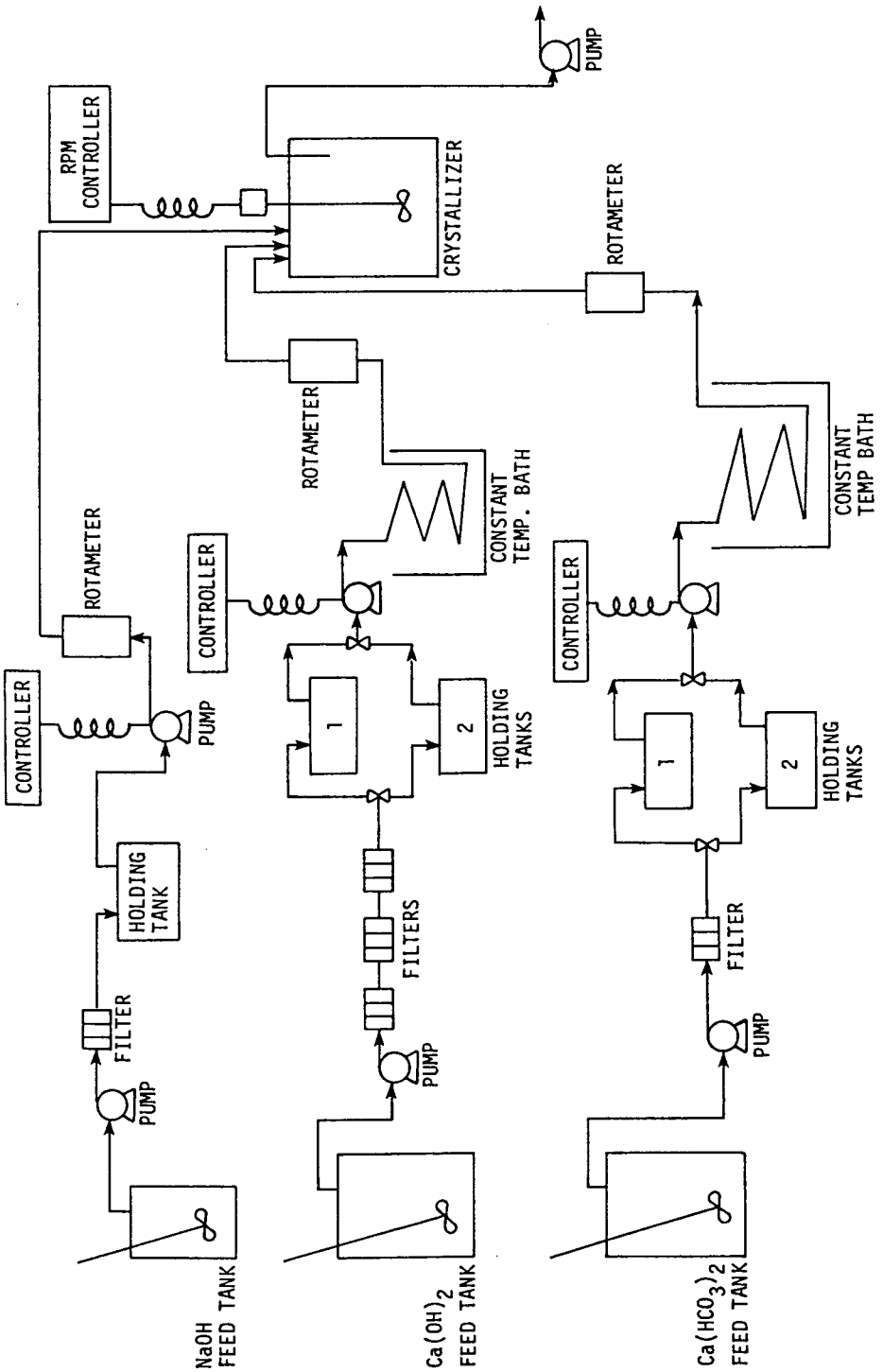

Fig. 5. Experimental equipment flow diagram

Figure 6a. Experimental equipment

Figure 6b. Experimental equipment

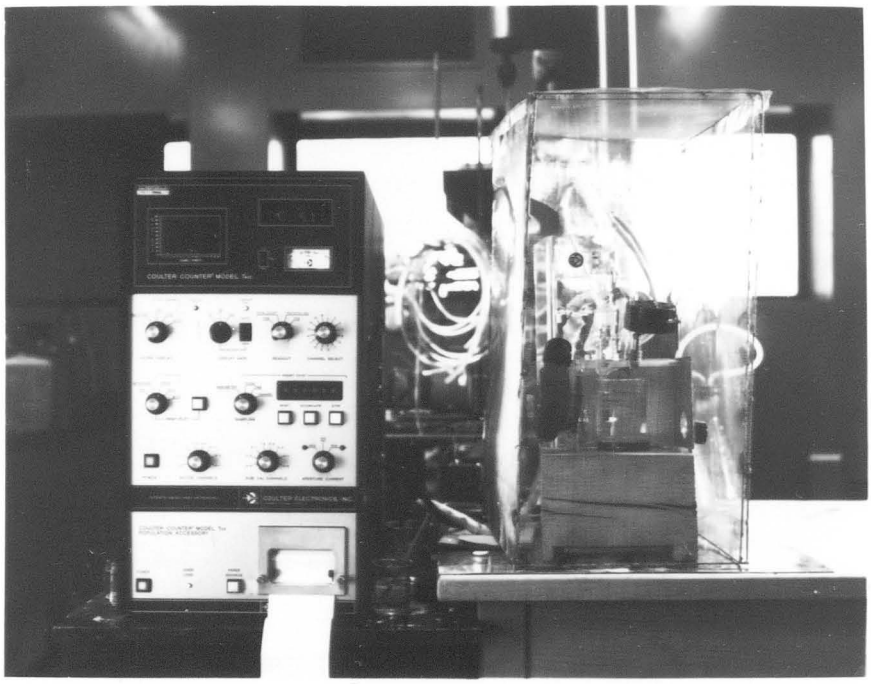

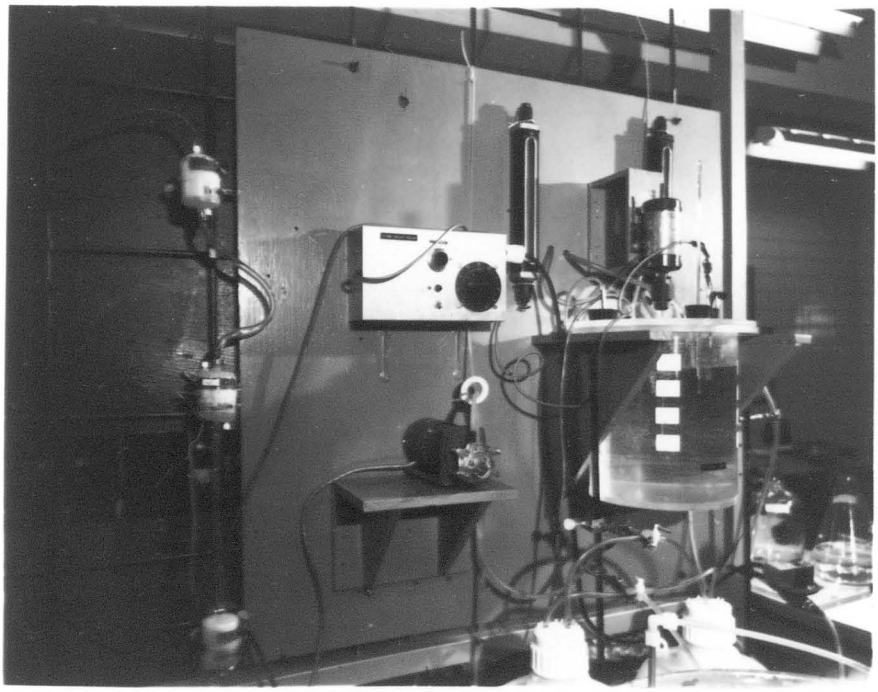

Figure 7a. Experimental equipment

Figure 7b. Experimental equipment

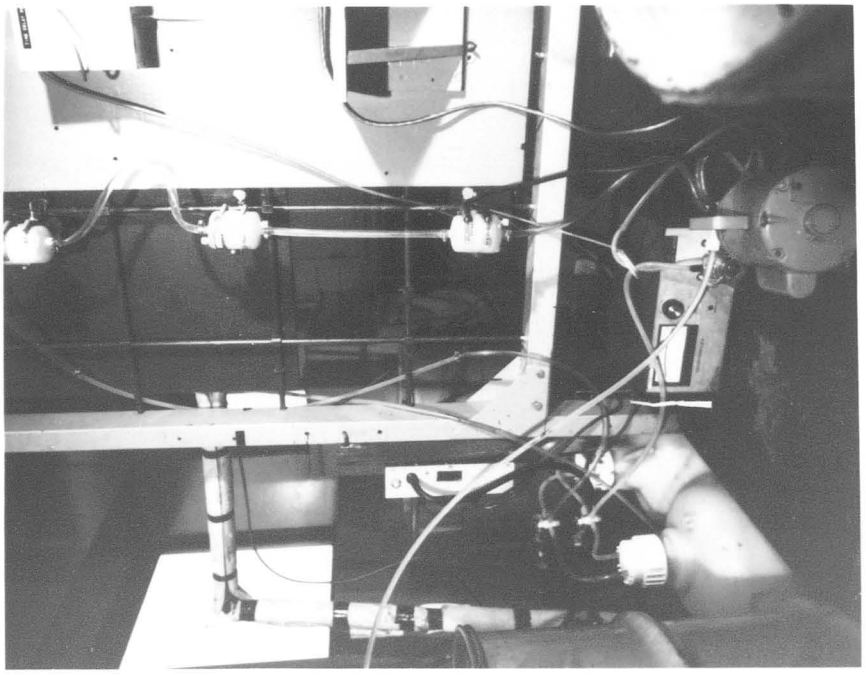

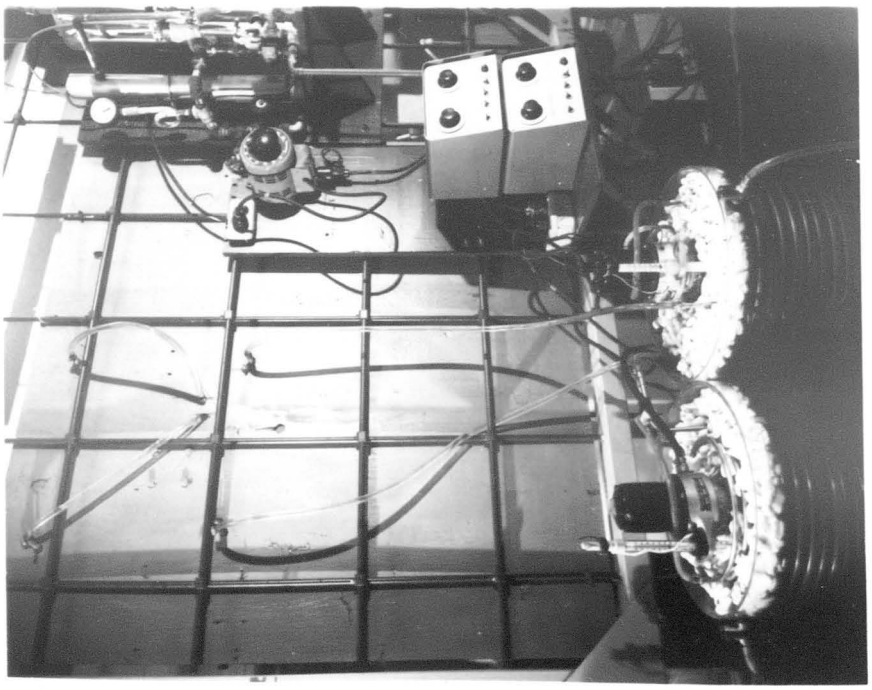

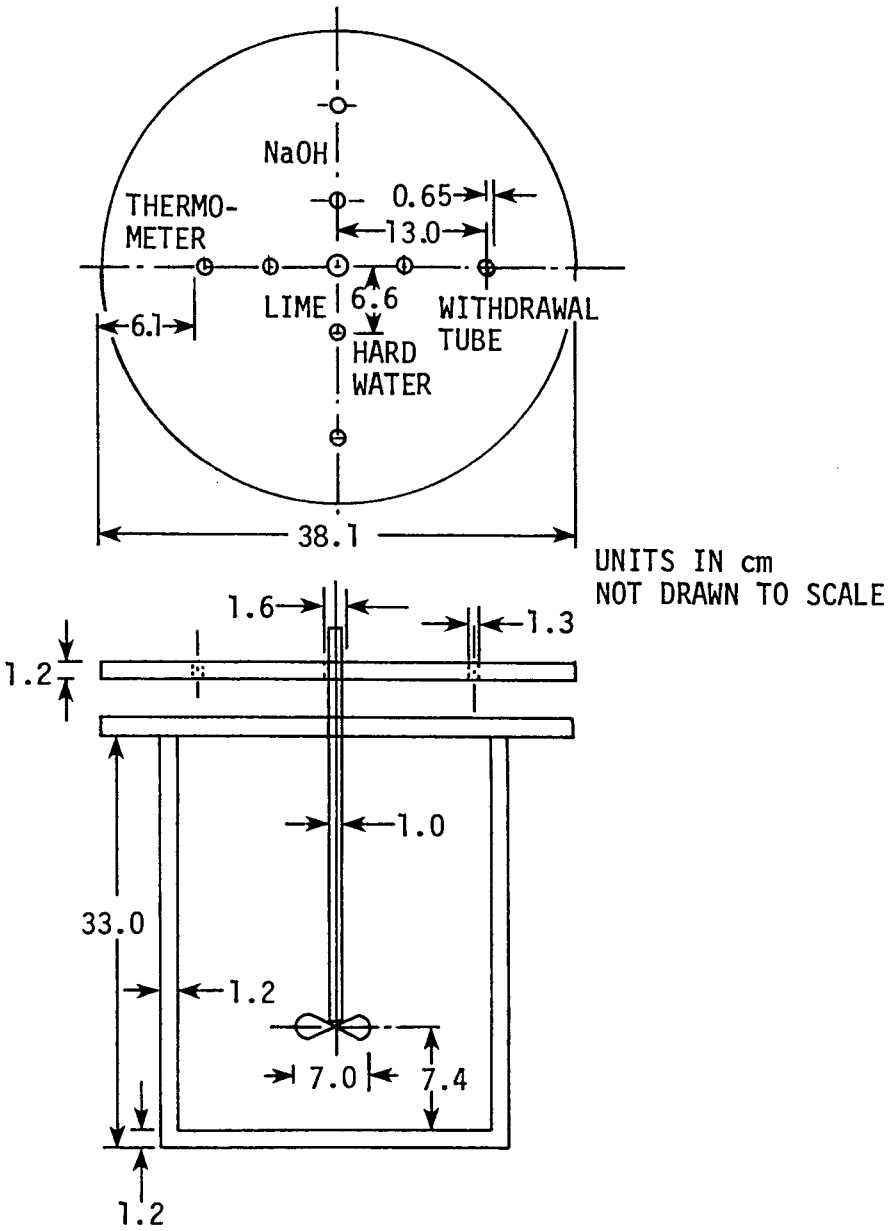

Fig. 8. Crystallizer

electrolytic solution containing particles through an aperture. One electrode is located inside the aperture tube, while another is placed in the crystal solution outside the tube. When solution is drawn through the aperture, a constant electrical current is passed through the aperture. A particle entering the aperture tube causes a resistance change proportional to its volume. The counter amplifies, analyzes, and sorts these resistance changes into 16 channels.

The Model TAII allowed sampling of a specified volume (0.5, 1.0, 2.0 ml), a specified particle count, or a specified time. The Coulter displayed the results in terms of a differential size distribution or a cumulative size distribution. The population accessory printed the results for subsequent analysis.

Feed and holding tanks

Lime and hardness feed tanks consisted of 55-gallon stainless steel tanks, while a 30-gallon stainless steel tank was used for the NaOH feed tank. Lightin 10X mixers were used to dissolve feed tank chemicals. A 21-inch impeller shaft with one blade was used for the NaOH, while 30-inch shafts with two and three blades were used for the lime and hard water tanks.

Stainless steel lids covered the feed tanks to prevent extraneous particles from falling into the tanks. In addition, plywood floats, drawn in Figure 9, were employed in the 55-gallon tanks to minimize CO_2 absorption by greatly decreasing the air-water interface area available for absorption. Legs were added to the

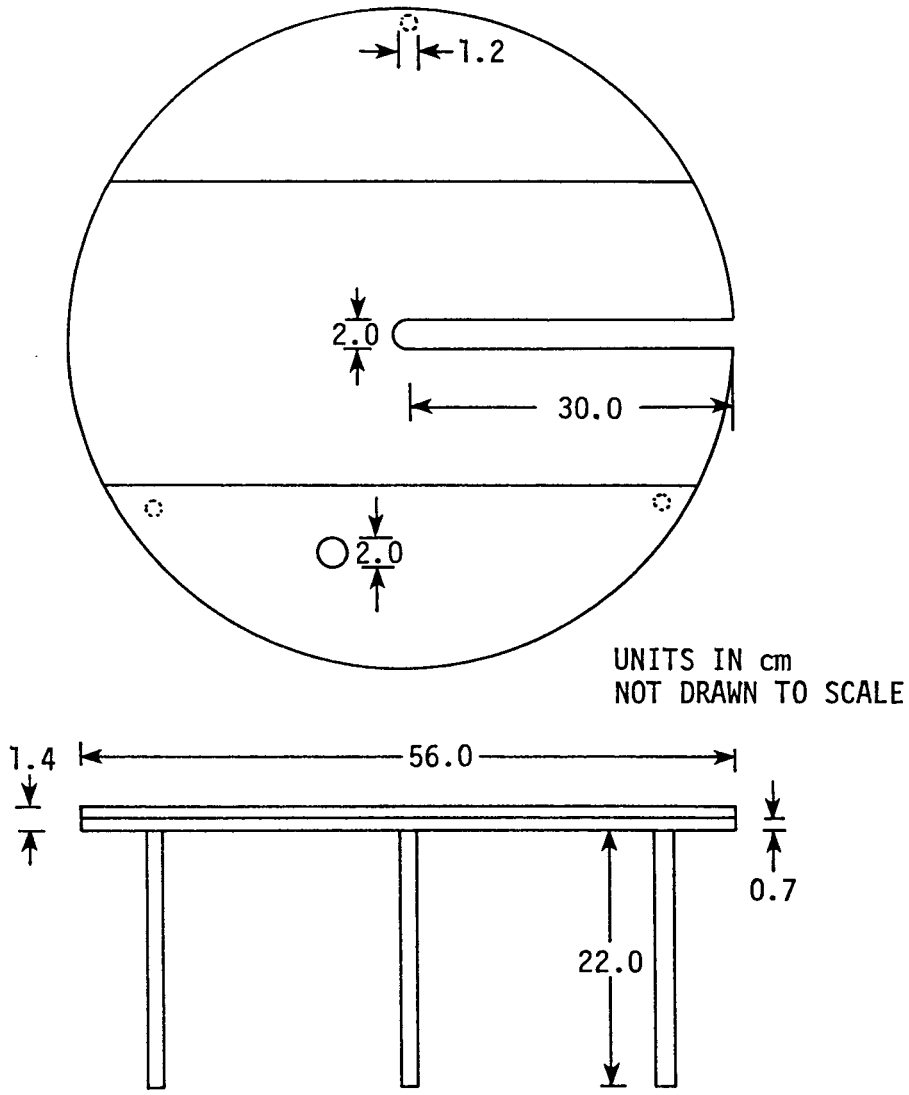

Fig. 9. Feed tank floats

floats to prevent interference with the impeller blades. These floats helped to hold both the lime and hardness feed concentrations nearly constant throughout the run.

Five-gallon polyethylene tanks served as holding tanks between the feed tanks and the reactor. The lime and hardness lines required two holding tanks each, while the NaOH line needed one holding tank.

In-line filters

The MSMPR model assumed no crystals entered the crystallizer. While all particles cannot be removed from the feed streams (27), these particles were minimized by filtering with Pall pleated membrane filters before storage in the holding tanks. 0.2 micron filters (Model 3001 AR) were used to filter the hardness and NaOH feed lines. Incomplete dissolution of $Ca(OH)_2$ necessitated a series of three filters of decreasing size. The first filter was 3.0 micron (Model DFA 3001 BPP), followed by 1.2 (Model DFA 3001 BN) and 0.45 (Model DFA 3001 AX) micron filters. This staging prevented lime plugging of any individual filter.

Pumps

The lime feed was pumped to the holding tanks with one side of a BIF Proportioneers Chem-O-Feeder Chemical Pump. The hardness feed was transported to the holding tanks with a Gorman-Rupp Industries Model M14251 pump. A Marathon Electric Model 5600 pump, Model 6QA 48C 171135B ECC was used to pump NaOH through the filter to the holding tank.

Cole-Parmer Masterflex variable speed drive pumps with solid-state controllers were employed to pump from the holding tanks to the reactor. The Masterflex pumps could be controlled much more closely than the other pumps. The silicon tubing needed for constant Masterflex flow rates would burst when connected to the in-line filters, preventing direct Masterflex pumping from the feed tanks. 7017 pump heads with a range of 84 to 1680 ml/min were used for the lime and hardness streams, while the NaOH line utilized a 7014 (7.5-150 ml/min) pump head. Model WZ1R031 pumps were used for lime and NaOH, while combination controller-pump Model 7565 pumped the hardness stream.

The other side of the BIF Proportioneers pump removed the treated water from the reactor. This flow rate could not be varied, so the reactor effluent line was placed at the air-water interface in the reactor to prevent drainage below the 16-liter level.

Constant temperature baths

The constant temperature baths in the lime and hardness lines consisted of stainless steel and copper tubing (for the feed streams and cold water circulation, respectively) immersed in a water-filled glass tank. Sargent Heaters and Circulators for Thermostatic Baths heated and circulated the water, while Sargent Thermocontrollers controlled the temperature.

pH meters

A Corning Model 130 pH meter with a sensitivity of ±0.001 pH units was used for most runs. Two glass electrodes and a glass temperature comsenator, all manufactured by Corning, were employed. A Beckman Model 72006 pH meter was used in a few early runs.

Flowmeters

Flowmeters indicated flow rates of each feed stream. Gilmont size 4 shielded flowmeters with a range of 10-850 ml/min revealed the lime and hardness flow rates, while a Gilmont size 13 flowmeter (2-300 ml/min) was installed in the NaOH line.

Balances

A Mettler H-15 balance with sensitivity of 0.1 mg was used for weighing the filter paper from suspension density measurements and small chemical quantities. Larger quantities were weighed with an Ohaus triple-beam balance.

Water supply

The water used in most runs was demineralized physical plant steam condensate. The condensate was collected in a 55-gallon polyethylene drum. A submersible pump was used to pump the water through Barnstead Q high capacity (Model DO503) and organic removal (Model DO513) water purification cartridges. The condensate was filtered with a cloth filter before entering the polyethylene drum and again with a 0.45 micron Pall filter after demineralization. A Barnstead Model SMO-SV still provided distilled water for early runs.

Other equipment

Three 50 ml burettes, two magnetic stirrers, and various pipettes were utilized in the titrations. A Hach Model 2510 Conductivity Meter measured the conductance of the filtered reactor effluent. A Blue M Electric Company oven dried the filter paper before suspension density measurements and evaporated the HCl in scale deposit determinations.

Experimental Conditions

Table 1 lists the experimental conditions for the various runs.

Table 1. Approximate experimental conditions

Series	Initial hardness, ppm as $CaCO_3$	T/P ratio	Residence times, min.
I	225	2.0	20, 30, 40
II	225	2.25	20, 30, 40
III	225	1.4	20, 30, 40
IV	350	1.6	20, 30, 40

The first three series were conducted at an initial hardness of 225 ppm as $CaCO_3$, well within the 100-700 ppm range for hard waters (11). The initial hardness in the fourth series was increased to determine how initial hardness level variations affect the softening process.

The first series was performed at a T/P alkalinity ratio of 2.0, where carbonate alkalinity is near a maximum (37). The second set was conducted at stoichiometric lime addition. This represents the lower limit of municipal lime treatment. The third series was performed at a pH of 11, near the upper limit of lime treatment. In addition to determining initial hardness level variation effects, the fourth series indicated predicative capabilities of an experimental correlation at an intermediate T/P ratio.

Varying the residence time provided supersaturation changes necessary to determine the kinetic order for each series. Forty minutes was the maximum residence time chosen due to the time involved to perform the experiment. The minimum residence time was twenty minutes for two reasons. First, the Chem-O-Feeder pump maximum flow rate is slightly less than the 400 ml/min lime flow in the twenty minute runs. A shorter residence time would drain the holding tanks before reaching steady state reactor conditions. Also, a shorter residence time would not allow performance of the analyses.

Experimental Procedure

The feed streams were prepared on the morning of the runs, except for the 40-minute residence time runs when the lime and hardness tanks were prepared the previous night. The hardness feed concentrations were 0.00225 mole/liter $Ca(HCO_3)_2$ for the first three series and 0.0035 mole/liter $Ca(HCO_3)_2$ for the fourth series. Twelve to fifteen percent excess lime concentrations were used for all runs except when the T/P ratio was 2.25. Sodium hydroxide concentrations included 0.0035 mole/liter (T/P = 2 and T/P = 2.25), 0.007 mole/liter (T/P = 1.6), and 0.025 mole/liter for the T/P = 1.4 series.

Feed tank preparation

Two hundred liter solutions were prepared for the lime and hardness feed streams, while 40 liters of NaOH solution were made up. These amounts provided excesses of the feed streams at the end of the runs, which were 17-20 residence times in length.

The lime and NaOH feed streams were prepared by dissolving reagent grade $Ca(OH)_2$ and NaOH in distilled water (roughly two liters for $Ca(OH)_2$, 0.2 liters for NaOH), adding these concentrated solutions to demineralized water in the feed tanks, and mixing for at least 10 minutes. Duplicate 50 ml aliquots of the solutions were titrated with 0.02 N hydrochloric acid to the phenolphthalein endpoint to determine the feed tank concentrations. The lime concentration was then adjusted, if needed, by adding $Ca(OH)_2$ or

distilled water. The NaOH concentration was less critical and needed no adjustment.

The hardness feed tank preparation was more complicated. Since calcium bicarbonate is unstable in solid form, it was formed by the reaction

$$CaCl_2 + 2\ NaHCO_3 \rightleftarrows Ca(HCO_3)_2 + 2\ NaCl \qquad (R15)$$

The desired anhydrous calcium chloride dosage was added directly to the feed tank and stirred for at least 10 minutes. Two 50 ml aliquots were titrated with 0.007 N EDTA solution as recommended by Diehl (11) to determine the calcium concentration. If needed, the feed tank was adjusted with $CaCl_2$ or distilled water and re-titrated until the desired calcium concentration was reached. An excess of about one gram reagent grade sodium bicarbonate was then added to the tank to force complete conversion of $CaCl_2$ to $Ca(HCO_3)_2$ and mixed for 10-15 minutes.

After the solutions were prepared, the floats were placed in the 55-gallon drums to decrease CO_2 absorption and the solutions pumped through the filters to the holding tanks. The feed tank mixers were turned off soon after the pumping began to further lessen CO_2 absorption in the tanks. Filling both lime holding tanks before starting the 20-minute residence time runs was necessary due to the low capacity Chem-O-Feeder pump. For the other runs, the holding tanks only required partial filling before start-up. One filling of the holding tank provided enough NaOH for the

entire run.

At least one hour before the start of the run, the filtered lime and hardness solutions were circulated from the holding tanks through the temperature baths and flowmeters and back to the holding tanks by Masterflex pumps. This circulation warmed up the pumps so that they could provide a more constant flow rate. These pumps were prepared for circulation by coating the pump rollers with caster oil and inserting silicon tubing between the rollers and the pump head.

Before the start of the run, three Whatman #42 9-centimeter-diameter filter papers were dried at 105°F for at least two hours. These were then cooled in a desiccator before use in suspension density measurement.

Flow rate determination

The flow rates were set so that the lime and hardness streams each provided one-half the flow rate needed for a given residence time. For example, the total flow rate for a 20-minute residence time run was 16000 ml/20 min, or 800 ml/min. The lime and hardness flow rates were each 400 ml/min. The NaOH flow rate, 5-30 ml/min, was added to this 800 ml/min so that the actual residence time was slightly less than 20 minutes.

Start-up

After the lime and hardness Masterflex pumps had been warmed up for 45-60 minutes, the run was started. Eight liters of demineralized water were added to the reactor to prevent initial

nucleation showers. Initial lime and hardness flow rates were determined with a graduated cylinder and a 0.1-second precision timer. When these flow rates were measured, the streams were introduced into the reactor, the agitator was started at a low speed and increased to 525 rpm as the reactor filled. The liquid level reaching the 16 liter mark in the reactor denoted the start of the run. The NaOH Masterflex pump was started, the flow rate measured, and the stream added to the reactor before the sixth residence time.

Operating conditions

The reactor temperature was maintained at 25 $\pm$0.3^{o}C by recording reactor and ambient temperatures each residence time and adjusting the temperature baths as necessary. Sodium hydroxide was added as needed to control effluent T/P alkalinity levels. Holding tank titrations were performed between one and three residence times and at the end of the run to determine average feed stream concentrations. Other measurements specified crystal size distribution, effluent alkalinity and hardness, suspension density (crystal weight per unit volume of reactor contents), and conductance of the reactor effluent. Equilibrium samples were collected for later analyses in several runs. In addition, the flowmeters were periodically checked to maintain feed stream flow rates.

Much of the precipitate formed during the experimental runs did not remain in suspension but adhered to reactor surfaces. Precipitate first collected on the glass impeller after one or two residence times. Buildup on the plexiglass reactor walls began

less than a residence time later. Peters performed tests that indicated scaling on plexiglass parts was linear with respect to time after this initial induction time (Robert W. Peters, Dept. of Chemical Engineering, Iowa State University, Ames, 1979, private communication).

Coulter counter measurements

The crystal size distribution (CSD) was measured with a Coulter Counter. The CSD sampling was begun after 11 residence times, when hardness, alkalinity, and conductivity data approached steady state. Five or six samples were taken during each run.

The counter was initially calibrated after ten residence times. The calibration procedure was taken from the Operator's Manual (7). A 280 micron diameter aperture tube was used for all runs. This size was necessary because a smaller aperture would plug with either one or a combination of particles. The accurate operating range for the aperture tube was 2%-40% of the aperture diameter (7), so 19.82 micron polystyrene beads were used. The counter was recalibrated 1-2 times during the run.

Before each CSD sample, a 200-300 ml filtered (0.2 micron filter) reactor effluent sample was analyzed to determine the number of counts associated with electrical noise. A background count increase of greater than a factor of two over the previous background count indicated recalibration was needed.

A CSD sample was taken soon after the accompanying background

sample. An aliquot of suspension was pipetted from the reactor and diluted with a known amount of filtered reactor effluent. This dilution, which varied from 1:1 to 22:1 depending on the number of particles in suspension, was necessary to prevent coincident particle passage in the aperture. The time between drawing suspension from the reactor and initial Coulter analysis was two-three minutes, due to diluting the sample, rinsing the pipette, and transporting the sample to the counter.

The counter was operated in the manometer mode with a 2.0 ml aliquot drawn through the aperture. This aliquot size provided an adequate number of particles for repeatable results.

Calcium carbonate scale deposited on the electrodes and the inside of the aperture tube. The outer electrode was brushed off after the CSD sample was analyzed whenever excessive scale was present. The aperture tube was flushed with 50-100 ml filtered reactor effluent before the background counts were taken. This flushing removed most of the scale, and the remaining scale was judged insignificant.

The accuracy of the counter was improved by averaging several readings. Each background sample was tested five or six times and the counts averaged. Each CSD sample was drawn through the aperture 7-10 times and 4-8 aliquots were averaged. Most CSD samples contained a few tests significantly higher and lower than most in the sample. All CSD samples during the run were averaged unless other

data (alkalinity, hardness, etc.) indicated steady state reactor conditions were not in effect for some samples.

Alkalinity measurements

The method used to determine alkalinities was reported in Standard Methods (40). The measurements were taken every 2-3 residence times. Erlenmeyer flasks (150 ml) were filled with filtered reactor effluent and stoppered so that no air-water interface existed in the flask. This prevented CO_2 absorption which would decrease the measured pH and affect the T/P alkalinity ratio.

A 50-ml aliquot was pipetted into a 150 ml beaker and titrated with a standardized 0.02 N hydrochloric acid to the phenolphthalein (pH = 8.3) and methyl red-bromcresol green (pH = 4.6) endpoints. The color changes involved are from pink to colorless for phenolphthalein and from blue to grey to orange in the mixed indicator. The initial pH of the sample was recorded along with pH readings after each acid addition. This titration usually took 30-45 minutes due to the time needed for the pH to equilibrate. Buffers of pH 10, 7, and 4 were used to standardize the pH meters.

Hardness titrations

Residual hardness titrations were performed at 3, 6, 9, 12, 15, and 18 residence times on filtered reactor effluent. The samples were collected in 250 ml Erlenmeyer flasks using the same procedure as for the alkalinity samples. The titrations were duplicated, with a third titration needed if the first two differed

by more than 0.1 ml.

The titrations were performed according to the procedure presented by Diehl (11). A 50-ml aliquot was treated with 1% potassium cyanide and 5 molar potassium hydroxide to mask the presence of other cations and titrated with standardized 0.007 N EDTA with a modified calcein indicator. The indicator changed from green to purple and needed a black background to accurately ascertain when the color changed. The titrations were performed rapidly to minimize CO_2 absorption which reversed the endpoint back to green. The EDTA was light sensitive and was stored in painted polyethylene bottles to prevent concentration changes.

Suspension density measurements

Suspension density measurements were taken at 7, 13, and 17 residence times. In a few runs, the second measurement was not taken, and in runs 31 and 32, only the 17 residence time measurement was taken.

The measurement was begun by weighing a dried filter paper and placing it in a Buchner funnel. The reactor effluent tube was pushed about halfway down into the reactor, a 500-ml sample of unfiltered reactor effluent collected in a graduated cylinder, the effluent tube returned to the 16-liter level, and the effluent filtered through the Buchner funnel. This was repeated three times for a total of two liters in the measurement. After the sampling, the filter paper was dried in the desiccator and weighed the following day.

Conductivity measurements

Conductivity measurements were taken each residence time to determine ionic strength and to help ascertain when steady state conditions had been reached. These readings were taken with filtered reactor effluent.

Equilibrium measurements

Measurements were taken to determine the equilibrium hardness levels in the reactor. Two liters each of filtered and unfiltered reactor effluent were collected at roughly 16 residence times. The unfiltered samples were collected in two 500-ml and one 1000-ml Erlenmeyer flask, while the filtered sample was collected in a 2000-ml Erlenmeyer. The flasks were stoppered so that they contained no air space. Hardness, alkalinity, and conductivity measurements were performed on the samples for several days after the run. All samples were refiltered through an 0.2 μm filter immediately prior to the equilibrium titrations.

Run shutdown and cleanup

After the necessary tests were completed, the run was shut down by measuring the final flow rates and draining the reactor. The reactor was placed in the laboratory hood overnight to dry. The following day the wall scale was dissolved with 500-100 ml 1 molar HCl, 100 ml of this hydrochloric acid was pipetted into a weighed 150-ml beaker, dried at 105^{o}C, and reweighed to ascertain the amount of wall scale produced during the reaction. All filters except the one used for equilibrium measurements were

backwashed with dilute HCl to dissolve trapped chemicals and rinsed with distilled water. The equilibrium titration filter was left unwashed to prevent reduced equilibrium pH readings due to trapped acid in the filter. The feed and effluent lines, as well as all tanks, floats, and impellers, were washed with dilute acid, rinsed with distilled water, and allowed to dry.

DATA ANALYSIS

Crystal Size Distribution Data

The crystal size distribution (CSD) data obtained using the Coulter Counter were the most important data acquired in this research. The CSD data allowed determination of the crystallization kinetics at the various reactor conditions.

As discussed in the Background section, the nuclei density n^o and the growth rate G can be obtained by plotting either ln n vs L or ln N vs L according to the equations

$$n = n^o \exp(-L/G\tau) \tag{E20}$$

and

$$N(L_1,\infty) = n^o G\tau \exp(-L/G\tau) \tag{E21}$$

Ln N vs L plots for Equation (E21) were used to calculate n^o and G because cumulative number $N(L_1^\infty)$ data above a size L_1 were more readily obtained from Coulter Counter data and more accurate than the population densities which were obtained from a numbers vs length plot,

$$n = dN/dL \tag{E19}$$

The determination of the slope $\Delta N/\Delta L$ at each length L adds an additional source of error. As Equation (E21) indicates, a plot of ln N vs L yields a straight line with slope $-1/G\tau$ and intercept ln $(n^oG\tau)$.

The nucleation rate B^o was calculated by Equation (23)

$$B^o = n^o G \tag{E23}$$

after the values for n^o and G for a CSD sample were found.

The CSD data were analyzed by first averaging the counts in each channel for 4-6 aperture tube aliquots of each filtered reactor effluent sample taken immediately before the CSD sample. This procedure ascertained the extent of background noise present in the system.

After the background sample was taken, 6-10 2.0-ml aliquots of the CSD sample were drawn through the aperture tube. The counts in each channel of several aliquots were averaged to improve the accuracy of the counter data. Counts from an individual aliquot passed three tests before averaging with counts from other aliquots. The Operator's Manual (7) stated that, for a 280-μm aperture, the time needed to draw a 2.0 ml sample was 7.0 seconds. Aliquots deviating more than 0.2 seconds from this time were not included in the averaging. Most aliquots in a sample centered around a given value of total counts. Aliquots with significantly higher or lower total counts than the majority of aliquots were rejected. In addition, aliquots with a size distribution greatly different from the other aliquots in the sample were not averaged.

After the suitable aliquots were averaged, the background counts in each channel were subtracted from the CSD counts to obtain the corrected counts in each channel. The number of particles

in each channel was calculated from the corrected counts:

$$\text{particle number} = (\text{number of corrected counts})\left(\frac{1}{\text{2.0-ml aliquot}}\right)(\text{total dilution}) \qquad \text{(E31)}$$

where the total dilution, for example, is 11 for a 10:1 dilution of CSD sample with filtered effluent (7). The particles per channel were added together from the largest size range down until the smallest size range is included to determine the cumulative numbers larger than the various size range. Tables 2 and 3 list raw and corrected Coulter data for two CSD samples in Run 20, and Figure 10 is a ln N vs L plot for the first sample.

Of the 16 channels in the Coulter Counter, the first two are unavailable for particle sizing because the channels represent sizes smaller than 2% of the aperture diameter. In addition, channels with less than ten corrected counts were not used.

Several CSD samples were taken during each experimental run. Nucleation and growth rates from the samples were averaged to obtain global nucleation and growth rates for the run, providing two criteria were met:

(1) The nucleation and/or growth rates for a particular sample did not vary by more than a factor of two from the other CSD samples.

(2) Hardness and alkalinity data remained roughtly constant throughout the sampling period.

In nearly all runs, at least three CSD samples were averaged together. In many runs, all CSD samples were included.

Table 2. Coulter counter data for run 20

Residence time	Dilution	Channel	Coulter counts	
			Aliquot 1	Aliquot 2
12.2	8:1	3	249	255
		4	201	199
		5	208	225
		6	180	196
		7	146	128
		8	97	130
		9	54	59
		10	32	28
		11	10	16
15.9	3:1	3	1075	1061
		4	722	740
		5	581	623
		6	471	413
		7	279	301
		8	165	227
		9	81	111
		10	45	54
		11	24	22
		12	4	8

Aliquot 3	Aliquot 4	Aliquot 5	Aliquot 6	Aliquot 7	Background count
231	246	265	235	256	7
224	209	249	234	215	4
225	227	214	196	230	2
196	166	203	194	169	3
152	167	164	174	172	2
115	103	113	100	107	1
57	61	60	67	62	0
31	34	41	29	28	0
20	13	14	13	13	0
1054	1135	1037	1064		10
727	769	798	732		5
596	551	616	536		4
463	394	437	430		2
311	280	295	324		2
173	199	187	193		0
104	98	79	112		1
41	46	52	63		0
25	21	21	19		0
14	16	10	10		0

Table 3. Corrected counter data for run 20

Residence time	Channel	Crystal length L_1, μ	Differential particle number number/ml	Cumulative particle number number/ml
12.2	3	8.50	1084.5	5512.5
	4	10.71	967.5	4428.0
	5	13.49	972.0	3460.0
	6	17.00	823.5	2488.5
	7	31.42	702.0	1665.0
	8	26.98	486.0	963.0
	9	34.00	270.0	447.0
	10	42.84	144.0	207.0
	11	53.97	63.0	63.0
15.9	3	7.86	2122	6980
	4	9.91	1502	4858
	5	12.48	1158	3356
	6	15.73	866	2198
	7	19.82	592	1332
	8	24.97	382	740
	9	31.46	194	358
	10	39.64	100	164
	11	49.94	44	64
	12	62.92	20	20

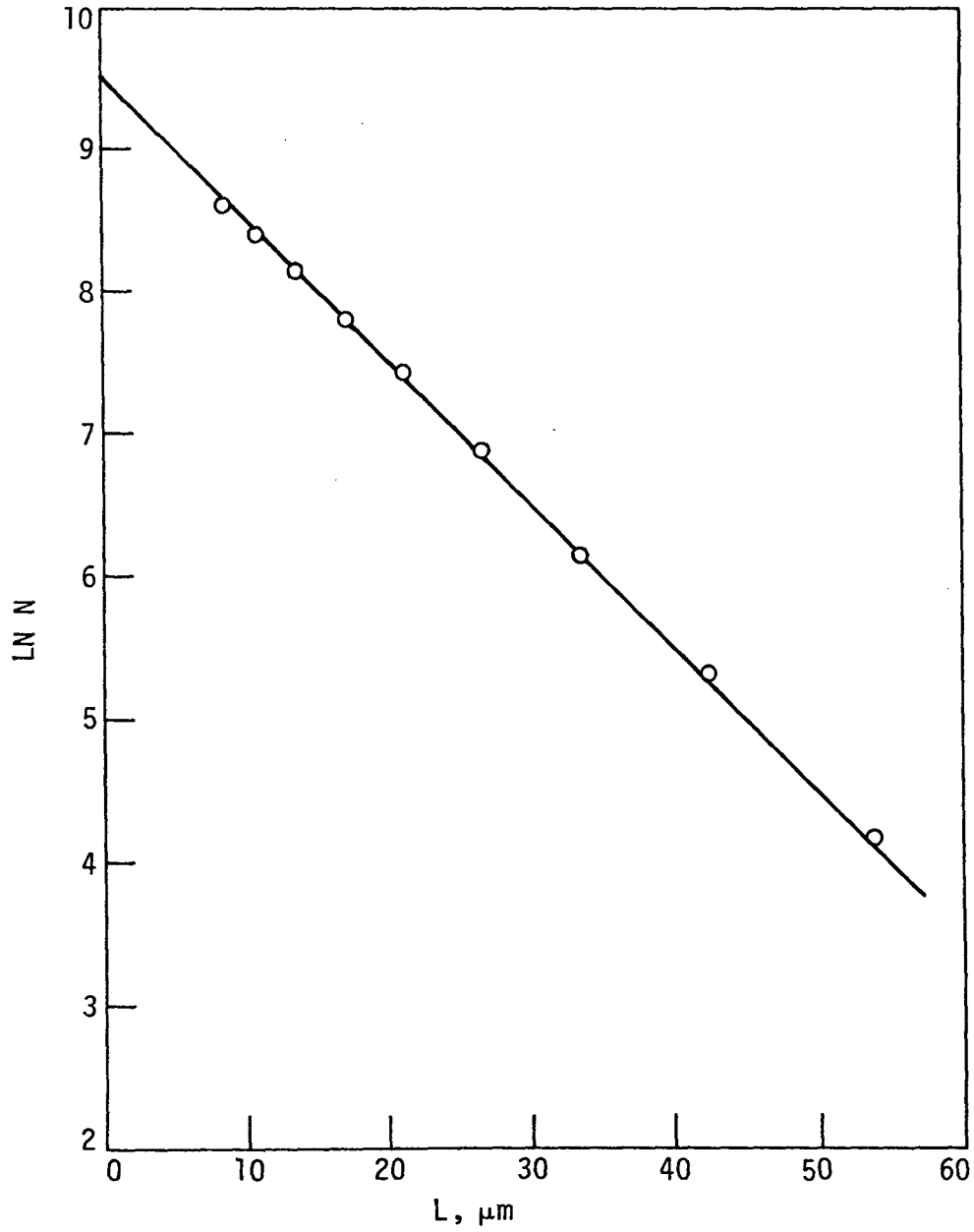

Fig. 10. Ln N vs L plot for run 20 at 12.2 residence times

Calcium Hardness Data

Calcium hardness levels were determined by titration with EDTA solutions of known concentration. The calcium hardness was calculated by (11):

$$\begin{matrix} Ca^{++} \text{ hardness,} \\ \text{ppm as } CaCO_3 \end{matrix} = \frac{(M \text{ EDTA})(\text{ml EDTA})(50{,}000\ ^{mg/l}/\text{equiv.})(2 \text{ equiv/mole})}{\text{sample volume (ml)}} \tag{E32}$$

The titration indicates the amount of EDTA solution needed to complex the calcium ions. All other quantities are known. The sample volume was always 50 ml.

The softening efficiency was calculated by subtracting the reactor effluent hardness from the initial reactor calcium level, dividing the difference by the initial hardness, and multiplying by 100. Since the crystal size distribution measurements were considered the most critical of this research, the final hardness level was ascertained by averaging the calcium levels from titrations performed during the Coulter Counter sampling. Since the $Ca(OH)_2$ and $Ca(HCO_3)_2$ feed streams both contain calcium hardness, a more complicated expression was used to calculate the initial calcium level:

$$Ca^{++}_{in} = \frac{([Ca^{++}]_h Q_h + [Ca^{++}]_1 Q_1)_i + ([Ca^{++}]_h Q_h + [Ca^{++}]_1 Q_1)_f}{(Q_h + Q_1)_i + (Q_h + Q_1)_f} \tag{E33}$$

where the subscripts h, 1, i, and f indicate hard water stream, line stream, initial conditions, and final conditions.

Alkalinity Data

Alkalinity samples were titrated with standardized hydrochloric acid after recording the effluent pH. Again, samples taken during Coulter Counter sampling were averaged to find the alkalinity conditions for the run.

The total alkalinity, expressed as mg/l $CaCO_3$, was calculated according to Standard Methods (40):

$$T = \frac{(\text{ml acid to reach second endpoint})(N_{HCl})(50{,}000\ \text{mg/l/equivalent})}{\text{sample volume (ml)}} \qquad \text{(E34)}$$

The phenolphthalein alkalinity was calculated using Equation (E34) by substituting the amount of acid needed to reach the first endpoint.

The hydroxyl, carbonate, and bicarbonate alkalinities were calculated using the effluent pH and total and phenolphthalein alkalinities (36):

$$OH,\ \text{mg/l as } CaCO_3 = 10^{(pH - 14.00)}\ 10{,}000 \qquad \text{(E35)}$$

$$CO_3 = 2(P\text{-}OH) \qquad \text{(E15)}$$

$$HCO_3 = T\text{-}OH\text{-}CO_3 \qquad \text{(E36)}$$

The indicators used for the endpoints were not sharp; therefore, pH was used to determine the endpoints. For runs with the Beckman pH meter, pH was plotted as a function of the amount of acid added. The endpoints were designated by the inflection points of the pH-ml acid curve. The Corning pH meter readings were judged

sufficiently accurate to assume the endpoints occurred at exactly pH = 8.30 and pH = 4.60, respectively.

Suspension Density Data

The suspension density was determined in two ways; direct filtering of reactor effluent and by a calcium mass balance. The low suspension densities involved (0.1-0.2 g/l) made these determinations difficult; hence, these data were considered the least accurate obtained in this research. The actual average suspension densities were most likely between the values obtained using the two methods for a particular run.

Filtering

From one to three two-liter reactor effluent samples were filtered as described in the Experimental Section. The suspension densities were reported as grams calcium carbonate per liter suspension. All sample values were averaged to compute the suspension density for a particular run. The values usually decreased markedly as the run progressed. Therefore, the values obtained by this method were considered lower than the actual suspension density. Other possible error sources were inaccurate weighings, loss of crystals, and crystallization during filtering.

Mass balance

The molar calcium balance for this system is:

$$M_T = \frac{([Ca^{++}]Q_{Ca^{++}})_{in} - ([Ca^{++}]Q_{Ca^{++}})_{out}}{Q_{Ca^{++}out}} - \frac{D_T}{V_T(100)} \qquad (E38)$$

where: in = inlet

out = outlet

Q = volumetric flow rate, l/min

D_T = total reactor wall deposition, gms

V_T = total reactor throughput volume, l

M_T = suspension density, g/l

100 = calcium carbonate molecular weight

The last term represents the wall scale accumulated on the reactor walls. The scale deposition was assumed linear with time. Flow rate variations of 3-5% during the run were common. Inlet concentrations decreased by roughly the same amount by the end of the run. The outlet calcium concentrations calculated during the Coulter sampling were usually 10-20 ppm (15-30%) lower than the calcium outlet concentrations before the Coulter sampling. For these reasons, the suspension densities determined by this method may have been as much as 10% above the actual densities.

Mass Balances

Several ionic species existed in the water softening system studied in this research. Mass balances were calculated for the calcium ion and the carbonate-bicarbonate ion combination. These

balances provided a check on the combined accuracy of the various analytical procedures.

A calcium mass balance must account for calcium in the lime and hard water feed streams, all calcium carbonate crystals on the walls and in the suspension, and unreacted calcium ions in the reactor effluent. The molar calcium balance over the entire course of the run is represented by:

$$\text{in} = \text{deposition} + \text{suspension} + \text{unreacted ions}$$

$$(Q_l+Q_h)_{in}[Ca^{++}]_{in} +_T + (D_T + M_T V_T)/100 + [Ca^{++}] +_T \qquad \text{(E39)}$$

where: $+_T$ equals the total time of the run. Calcium balance closure was calculated by:

$$\% \text{ calcium closure} = \left(\frac{Ca^{++}_{out} - Ca^{++}_{in}}{Ca^{++}_{in}}\right) \times 100 \qquad \text{(E40)}$$

The carbonate and bicarbonate ions were balanced together because the bicarbonate reacted to form calcium carbonate. The feed streams contained essentially no carbonate ions. In addition to the calcium carbonate precipitate found on reactor surfaces and in suspension, the reactor effluent contained both carbonate and bicarbonate ions. Equation (E41) was employed to calculate the carbonate-bicarbonate balance:

$$HCO_3^- \text{ in} = HCO_3^- \text{ eff} + CO_3^= \text{ eff} + CO_3^= \text{ dep} + CO_3^= \text{ susp} \qquad \text{(E41)}$$

$$[HCO_3^-]_{in}(Q \text{ hard water})_{in} +_T = [HCO_3^-]V_T + [CO_3^=]V_T + (D_T+M_T V_T)/100$$

The carbonate-bicarbonate closure percentage was calculated by

$$\% \text{ closure} = \left(\frac{CO_{3\ out}^{=} + HCO_{3\ out}^{-} - HCO_{3\ in}^{-}}{HCO_{3\ in}^{-}}\right) \times 100 \qquad \text{(E42)}$$

Conductivity Data

The conductivity data were used to determine reactor effluent ionic strengths and when steady state conditions had been reached. The conductance is proportional to the amount of dissolved solids present in the effluent. The ionic strengths were calculated with an equation fit from calibration of the conductivity meter with solutions of known ionic strengths:

$$\text{conductance} = -5.423 \times 10^{6}\ I^{3} + 1.853 \times 10^{5}\ I^{2} + 1.160 \times 10^{5}\ I + 1.648 \qquad \text{(E42a)}$$

Where the conductance was the average of all conductance readings taken after 10 residence times. The conductance usually varied by less than five percent after 10 residence times, indicating roughly steady state conditions had been reached.

RESULTS AND DISCUSSION

Crystal Morphology

The three major crystalline forms of calcium carbonate are calcite, aragonite, and vaterite (10, 44). Calcite crystals are rhombic in shape, aragonite needle-like, and vaterite disk-like (10) or spherulitic (44). Calcite and aragonite are the most common forms (44).

A scanning electron microscope (SEM) was used to analyze the morphology of the calcium carbonate crystals formed during several runs. The crystals were taken from suspension density measurements and reactor wall depositions. An X-ray diffraction analysis was performed on reactor wall scrapings from one run.

Figures 11 and 12 are photomicrographs of typical crystals formed during the first two series of experiments, where lime dosages are relatively low. Crystals similar to the needle-like (dendritic) forms in these figures have been called vaterite by previous researchers in this laboratory (31, 37), in agreement with work performed by Wray and Daniels (44). Dedek (10), however, presented pictures of the three crystal forms which show the dendrites in Figures 11 and 12 more closely resemble aragonite. X-ray diffraction analysis on reactor wall scrapings and suspension density crystals in Run 19 confirmed most wall scraping and essentially all suspension crystals are aragonite, with the remainder being calcite.

A shift in the crystal size distribution toward the smaller

Figure 11. Photomicrograph of calcium carbonate crystals taken from Run 17 suspension at 17.7 residence times (1500X)

Figure 12. Photomicrograph of calcium carbonate crystals taken from Run 7 suspension at 17.2 residence times (2500X)

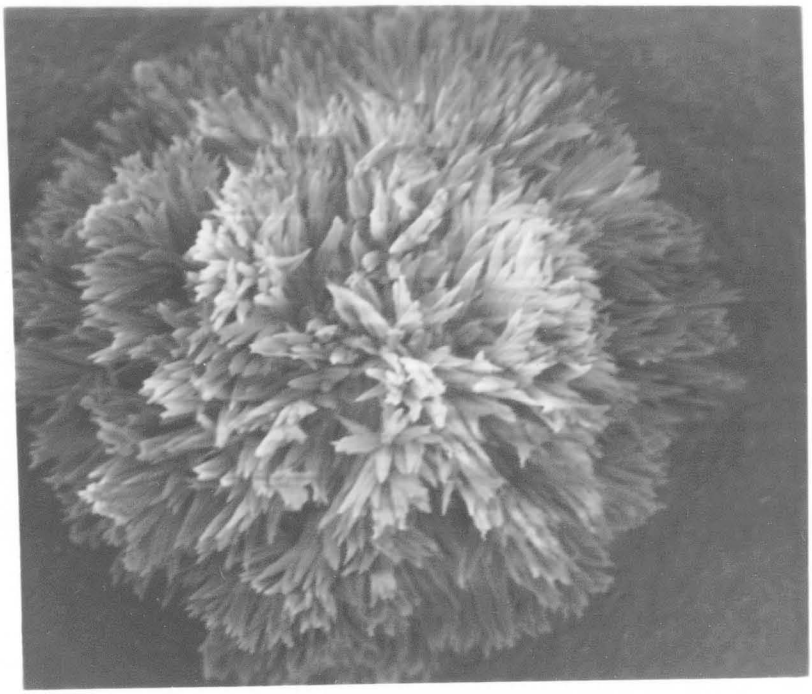

sizes occurred in the latter part of most runs in the last two series, where lime treatment levels were higher. The habit of suspension density crystals of most runs in these two series was inspected to determine whether the habit changed whenever the shift occurred.

No size shift took place in Run 23, the 40-minute residence time run with 225 ppm initial hardness and a T/P ratio of 1.4. SEM analysis (not shown here) indicated the crystals remained virtually all aragonite during the run. In a 20-minute residence time run of that series, Run 25, a size shift occurred between 16 and 18 residence times. Figure 13, an SEM photomicrograph taken of crystals removed from suspension at 13 residence times, shows the vast majority of crystals are aragonite. Figure 14, taken at 17 residence times, indicates roughly equal amounts of rhombic calcite and aragonite are present in suspension. These figures imply that the crystal habit does indeed change as the size distribution shifts toward the smaller sizes.

In Series IV, with initial hardness 130 ppm higher than in Series III but lime dosage per ppm hardness less than Series III, the size shifting started earlier in the run and exhibited greater nucleation and growth rate changes than in Series III. Figure 15, taken of crystals removed from the reactor at 7 residence times in a 20-minute run (Run 29), shows virtually no aragonite crystals. Interestingly, a number of disk-like crystals, possibly vaterite, are also present. This was the only photomicrograph taken of

Figure 13. Photomicrograph at crystals taken from Run 25 suspension at 13.5 residence times (1000X)

Figure 14. Photomicrograph of crystals taken from Run 25 suspension at 17.3 residence times (1000X)

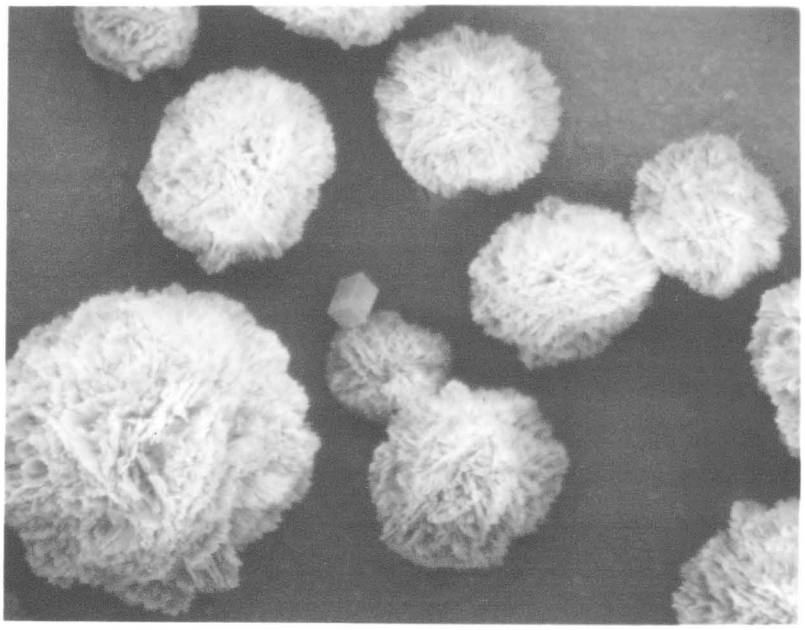

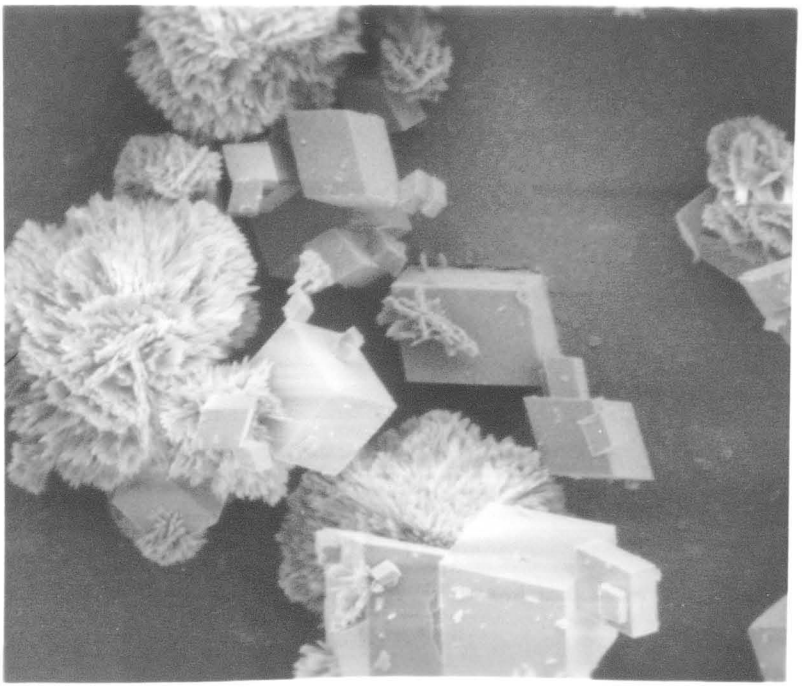

crystals removed so early in a run and the only one showing these disks. A photomicrograph of Run 30 (30-minute residence time) crystals at 13 residence times, nearly identical to one at the same point of Run 29, contain virtually all calcite crystals. Figure 17 shows that essentially no aragonite was present at 17 residence times in the 20-minute residence time run, typical of the samples at this point of the Series IV runs. These pictures imply that, after the CSD shifts, the crystal habit is not a function of residence time length.

Mullin (27) noted that well formed crystals are present only at low supersaturations, and that dendrites occur at higher supersaturations. Tables 6 and 8, presented in the Hardness Removal and Alkalinity Results subsections, show residual supersaturation (defined as the product of calcium and carbonate ionic concentrations minus the corrected solubility product) is smallest for runs in the fourth series, where all runs experienced a CSD shift. The CSD in all runs except the 40-minute residence time run in the third series also shifted. Since Run 23 (40-minute residence time) had the highest residual supersaturation in Series III, indications are that a critical residual supersaturation exists below which reasonably well-formed calcite particles develop and above which dendritic aragonite crystals predominate, and that this critical supersaturation may be a function of residence time. Further work is needed to determine more precisely this critical supersaturation level and the effect residence time length has on the tendency

Figure 15. Photomicrograph of crystals taken from Run 29 suspension at 7 residence times (1000X)

Figure 16. Photomicrograph of crystals taken from Run 30 suspension at 13.5 residence times (1000X)

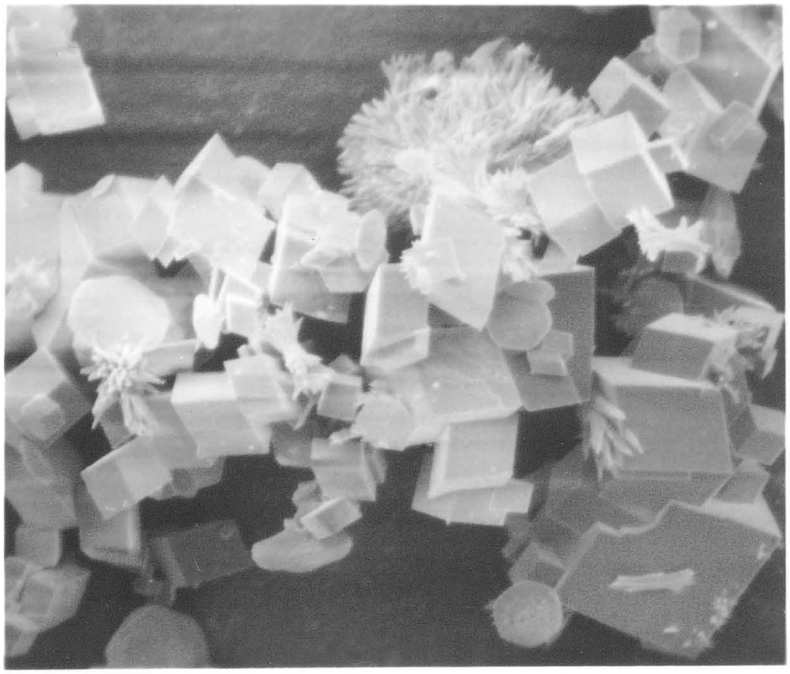

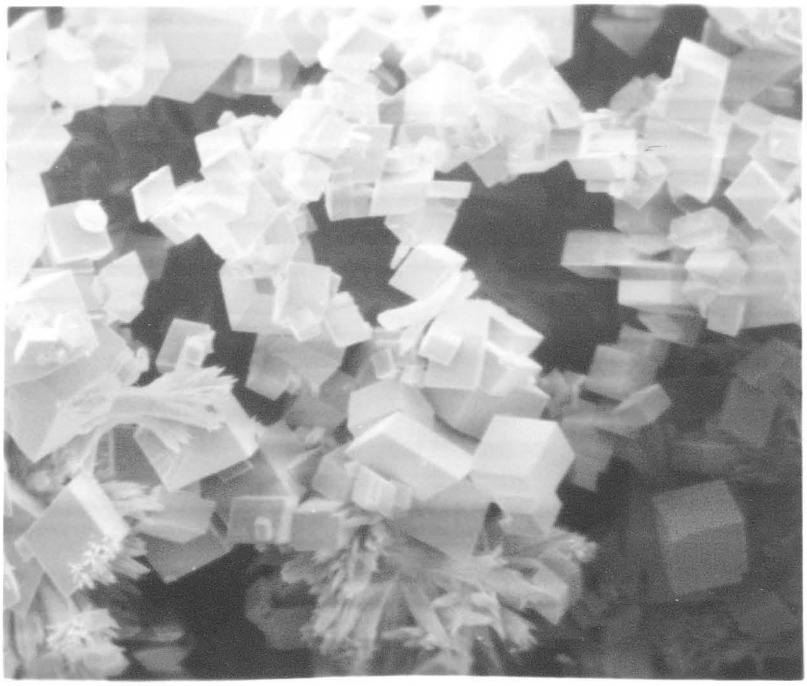

to shift to calcite.

Figures 18-20 show calcite crystals present at the reactor walls in Series I. Calcite was more prevalent at the reactor walls than in suspension in nearly all samples analyzed, possibly because calcite is the only thermodynamically stable form of calcium carbonate in solution (44). Wray and Daniels (44) noted that a 45°C solution of 30% calcite and 70% aragonite aged for two hours converted to 90% calcite. If the crystals were dried, however, the shift from aragonite to calcite ceased. A similar process may have taken place in this research, as the particles at the reactor walls remained exposed to solution much longer than the crystals removed during suspension density measurements.

Figure 20 shows an aragonite crystal with a flat side in a reactor wall scraping sample of Run 7. This indicates either crystal breakage during scraping or nucleation at the reactor surface. Since the scraping probably would not have caused such a clean break, it appears some nucleation did occur at the reactor wall.

Kinetic Measurements

Crystallization kinetics were determined by conducting experimental runs at 20, 30, and 40-minute residence time runs for three alkalinity distributions at about 225 ppm initial hardness (Series I-III) and one alkalinity distribution at roughly 350-360 ppm initial reactor hardness (Series IV). The residence time variations

Figure 17. Photomicrograph of crystals taken from Run 29 suspension at 17 residence times (1000X)

Figure 18. Photomicrograph of crystals taken from Run 11 reactor walls (300X)

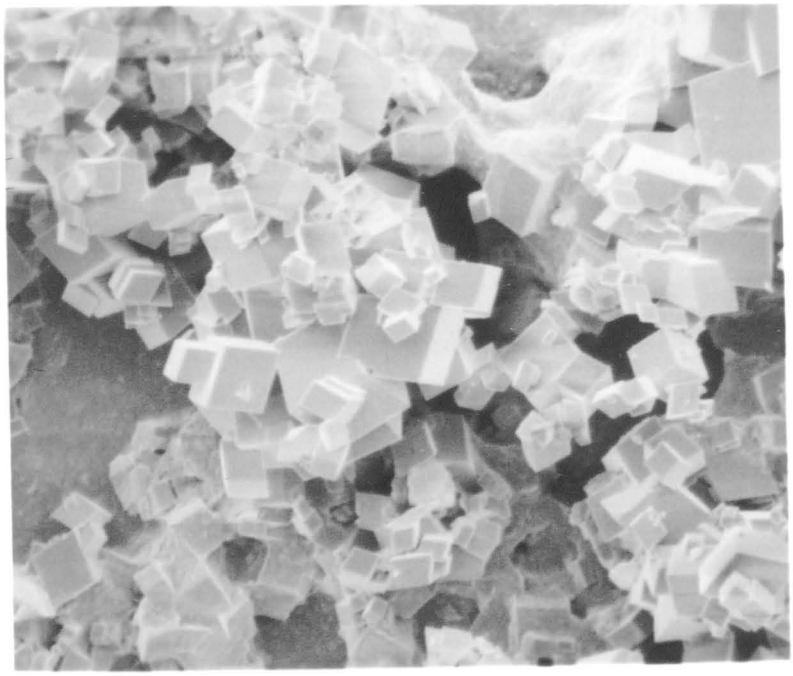

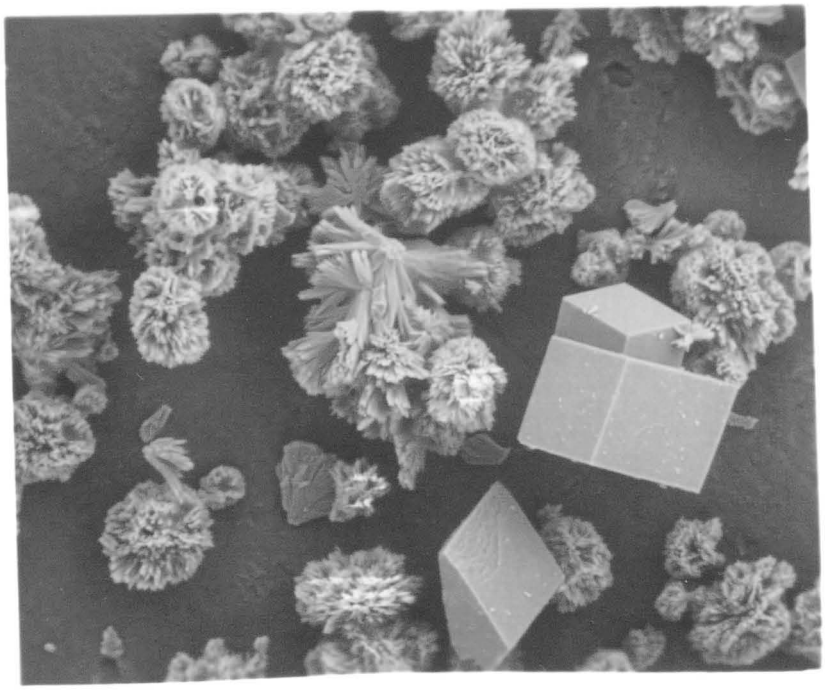

Figure 19. Photomicrograph of crystals taken from Run 11 reactor walls (1000X)

Figure 20. Photomicrograph of crystals taken from Run 7 reactor walls (500X)

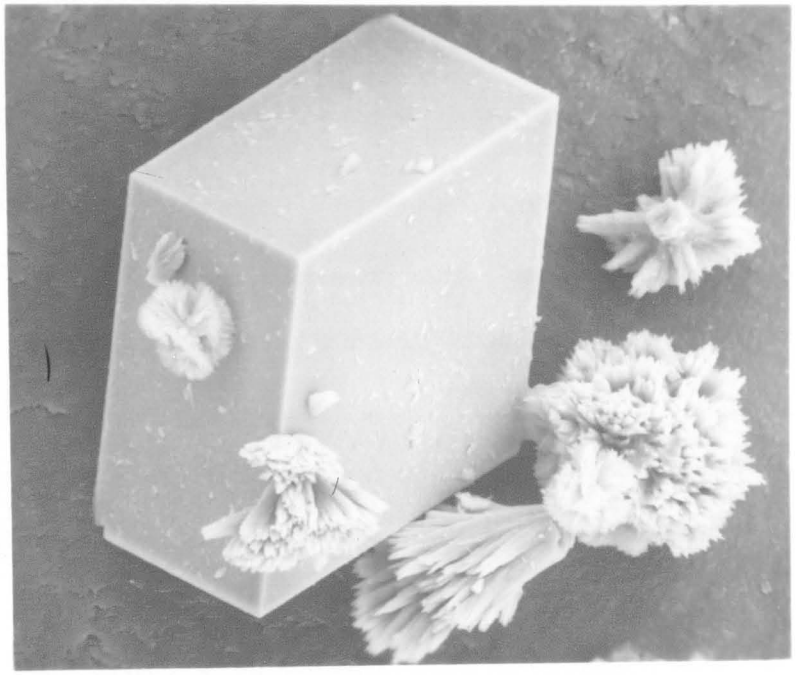

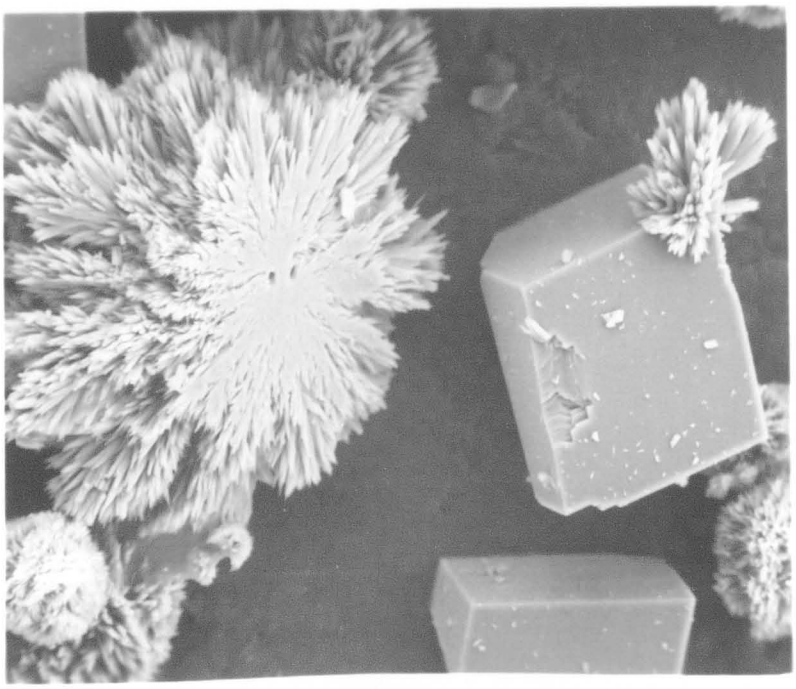

provided supersaturation changes for each set of initial conditions which produced changes in nucleation and growth rates. Nucleation rates were modeled as power law functions of growth,

$$B^o = k_N G^i \tag{E29}$$

as discussed in the Background section. When Equation (E29) is a valid model, a plot of ln B^o vs ln G produces a straight line with slope i and intercept k_N.

Kinetic data for individual runs are listed in Table 4, while kinetic order and coefficient values for the four series are listed in Table 5. The growth rates are the most critical values in Table 4, as the nuclei density (n^o), dominant size (L_D) and nucleation rate (B^o) values are all dependent on the growth rates, as described in the Data Analysis and Background sections.

Figures 21 through 24 are nucleation-growth rate plots for the four series. The kinetic expressions for the series are:

$$\text{I:} \quad B^o = 1.6 \times 10^3 \, G^{2.0} \tag{E43}$$

$$\text{II:} \quad B^o = 8.0 \times 10^2 \, G^{2.1} \tag{E44}$$

$$\text{III:} \quad B^o = 1.1 \times 10^5 \, G^{5.2} \tag{E45}$$

$$\text{IV:} \quad B^o = 7.3 \times 10^6 \, G^{5.8} \tag{E46}$$

Series I was conducted near maximum effluent carbonate conditions, as described by Schierholz (37), while Series II required the least amount of lime treatment (T/P = 2.25). The kinetic orders in these two series were not significantly different, but the coefficient in Series I

Table 4. Kinetic data for individual runs

Run	Series	τ, min	G, um/min	n^o, $\frac{\text{no.}}{\text{ml}\,\mu\text{m}}$	B^o, $\frac{\text{no.}}{\text{ml min}}$	L_D, μm
7		29.9	0.375	488	183	33.6
8	I	20.3	0.537	938	504	22.7
9		39.8	0.238	409	97.3	28.4
11	-	29.8	0.355	603	214	31.7
16		29.8	0.404	275	111	36.1
17		19.8	0.578	502	290	34.3
19	II	39.3	0.201	136	27.4	23.7
21		29.4	0.395	339	134	34.8
22	-	19.9	0.648	486	315	38.7
20		29.4	0.333	1260	419	29.4
23	III	38.5	0.307	664	204	35.4
25		19.7	0.435	2830	1230	25.7
26	-	18.9	0.421	3300	1390	23.9
29		19.5	0.293	20900	6130	17.1
30	IV	29.4	0.221	7600	1680	19.5
31		38.1	0.204	2950	601	23.3
32		29.4	0.244	6270	1530	20.8

Table 5. Kinetic order values

Series	i	k_N	Correlation coefficient, r	Average L_D	90% confidence intervals for "i"
I	2.0	1.6×10^3	0.978	29.1	±0.3
II	2.1	8.0×10^2	0.993	33.5	±0.4
III	5.2	1.1×10^5	0.982	28.6	±2.6
IV	5.8	7.3×10^6	0.951	20.2	±4.3

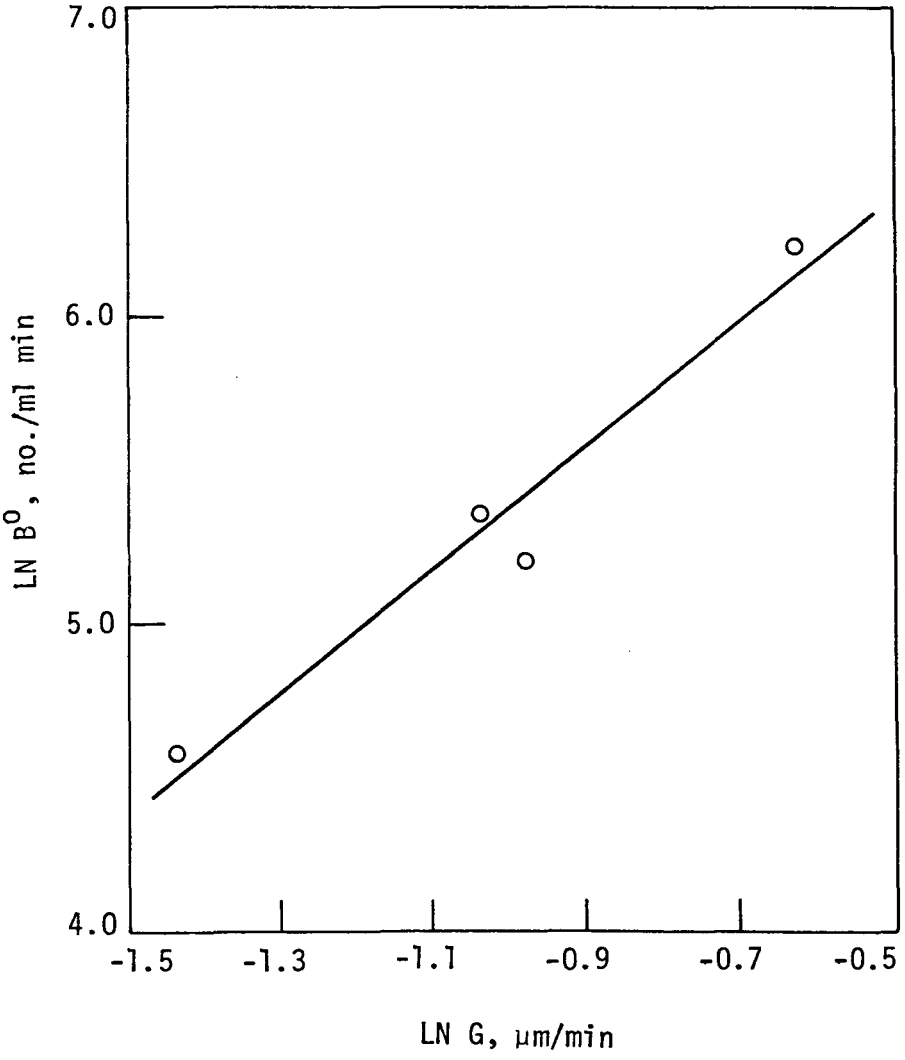

Fig. 21. Kinetic data for series I

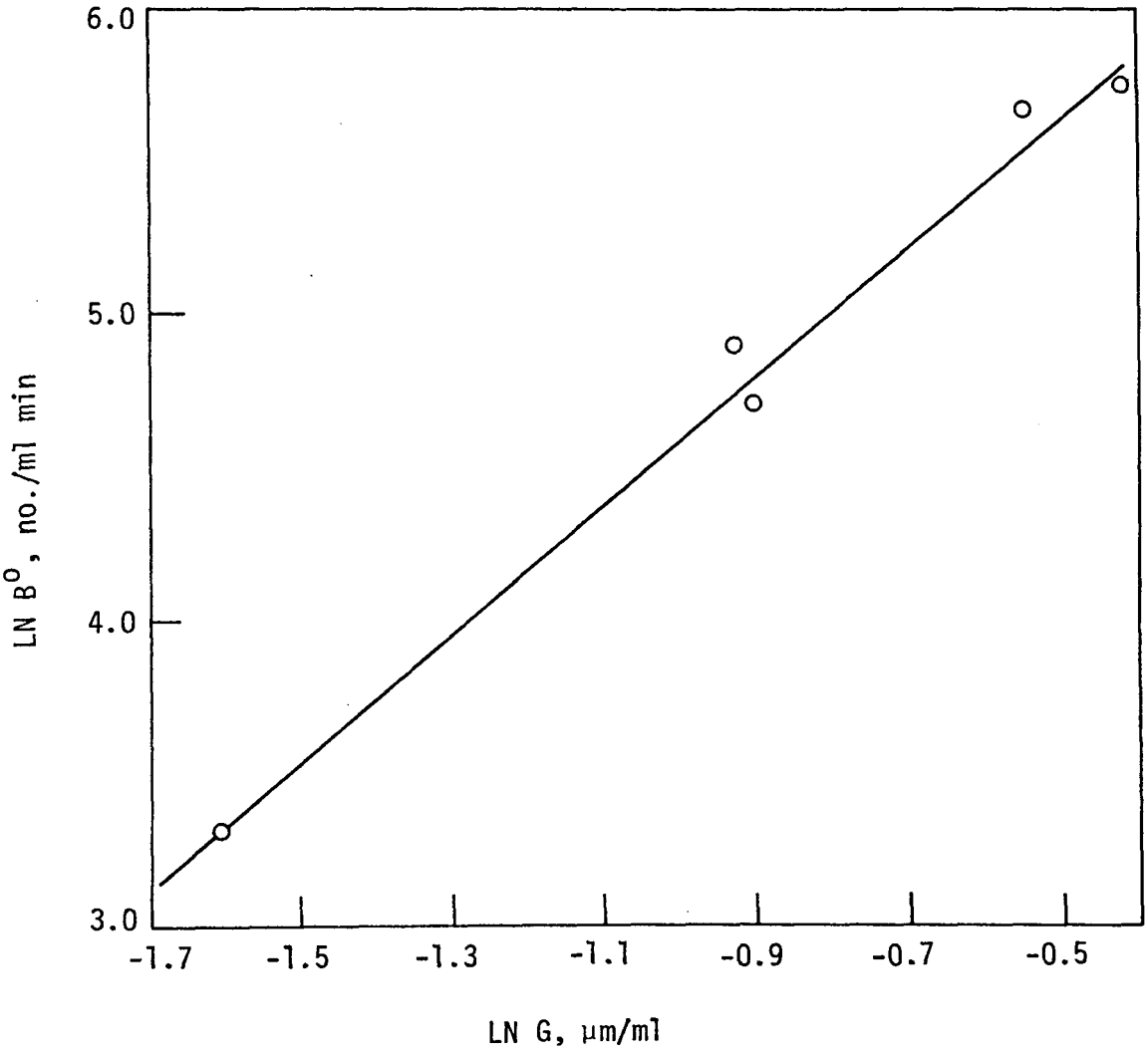

Fig. 22. Kinetic data for series II

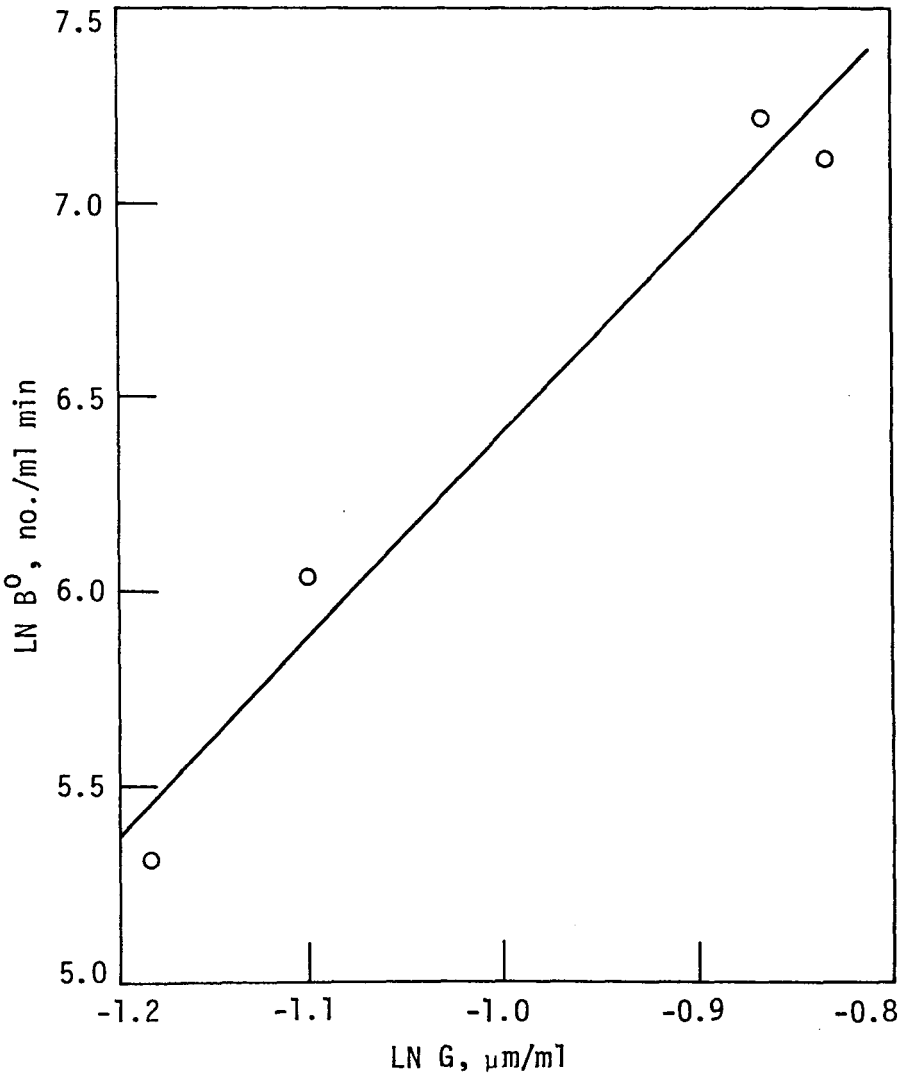

Fig. 23. Kinetic data for series III

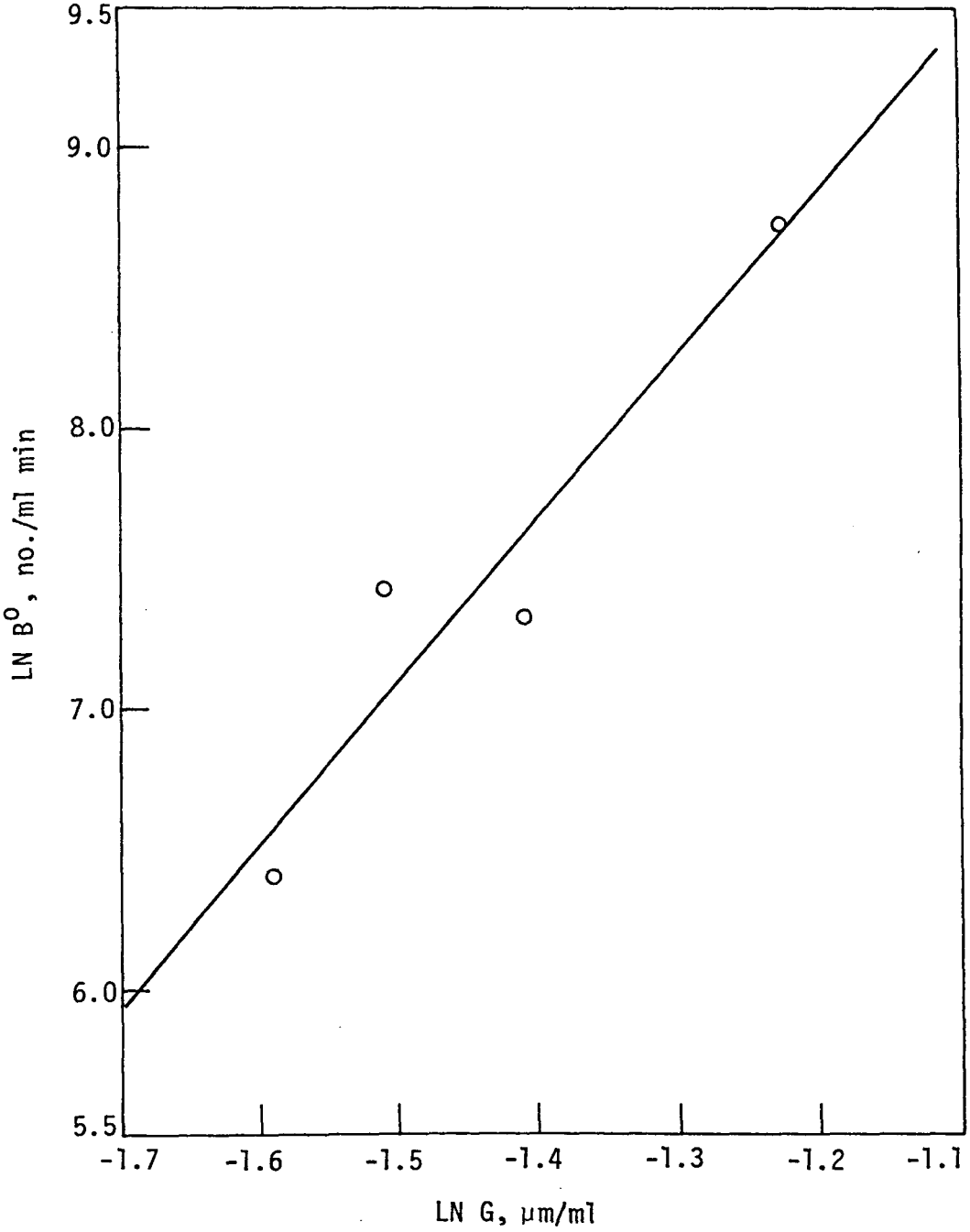

Fig. 24. Kinetic data for series IV

was twice that of Series II. The third series was performed at the highest lime treatment (pH = 11.0, T/P = 1.4).

Series IV produced surprising kinetic results. Kinetic results from Series I-III implied the kinetic order increased as pH increased whenever pH levels were above that of the carbonate alkalinity maximum. However, Series IV, with a lower pH than Series III, displayed a higher kinetic order than Series III.

Coulter Counter data and SEM photomicrographs indicated the CSD shifted toward the smaller sizes in Runs 20, 25, 26, 29, 30, 31, and 32. Coulter data shows the shift may have occurred in Runs 21 and 22, though no SEM photomicrographs are available at this time for these runs. The CSD shifted at 15-17 residence times for 225 ppm initial hardness runs, while the shift was first noticed at 13-15 residence times during Series IV runs. Whenever the CSD shifted, only Coulter Counter samples taken before the shift was seen were averaged to obtain global nucleation and growth rates for the run because it was believed the shifting violated the MSMPR assumption of steady state reactor conditions. Even with this precaution, photomicrographs show that calcite size distributions were measured in Series IV runs, while aragonite distributions were found in Series I-III runs.

This difference in crystal habit makes any comparison between Series IV and the three lower initial hardness series quite risky. For example, the calculated growth rates obtained in Series I-III are significantly higher than those at equivalent residence times

in Series IV. This does not necessarily mean the actual growth rates are higher for the aragonite runs. The Coulter Counter measures a change in resistance proportional to the volume of the particle passing through the aperture. The photomicrographs show that, for the same amount of mass, an aragonite crystal is much larger than a calcite crystal but has void space between the needles protruding from the center of the aragonite. Assuming the Coulter Counter measures the "projected" volume of the aragonite crystals (calcium carbonate + void space) and not just the volume of the calcium carbonate, the aragonite crystals appear larger than the calcite crystals; hence, the calculated aragonite growth rates are larger. In other words, less calcium carbonate must be deposited on an aragonite crystal than a calcite crystal to produce a one-micron increase in size. The same rate of calcium carbonate deposition on growing crystals may take place in both the aragonite and calcite systems.

The aragonite data of Series I-III show the kinetic order at high lime treatment is over twice as great as the kinetic orders at lower lime treatment, where T/P values are near 2.0. Since the growth rates at the longer residence times are nearly the same, this indicates many more crystals nucleate at the higher lime treatment. This is an example of how the driving force for crystal nuclearion varies as reactor conditions change. Dabir (8) and Peters (31) also found the kinetic order increases as softening agent dosage increased for other water-softening precipitation

reactions.

Much more variation was found in the kinetic orders in the three aragonite series in this research than was observed by Schierholz (37). The major reason for this increased variation is believed to be the reactor wall scraping by Schierholz to prevent crystal deposition which returned many particles to the reactor suspension. These returned crystals provided much surface area for crystal growth, thus holding the nucleation rate fairly constant from series to series. Hence, the kinetic orders found by Schierholz were more constant than those found in this study. Schierholz also studied precipitation from a different chemical system with higher T/P ratios, but kinetic order differences between Schierholz and this work due to the chemical system are considered minimal in comparison to the wall scraping effects.

The dominant size is important to softening plant designers because solid-fluid separations are aided by increased particle size. Randolph and Larson (33) defined the dominant size, L_D:

$$L_D = 3G\tau \qquad \text{(E47)}$$

The average dominant sizes of the first three series did not vary at the $\alpha = 0.05$ significance level. The dominant sizes were lower in Series IV due to the shift from aragonite to calcite crystal habit, causing a lower calculated growth rate (and dominant size).

Hardness Removal

Table 6 lists hardness and ionic strength data for the individual runs, and Table 7 contains the average values of each quantity in Table 6 for the four series. The hardness titrations were duplicated and varied by less than 0.10 ml (5%); hence the softening efficiency data were considered among the most accurate of this research.

The solubility product, $[Ca^{++}][CO_3^{=}]$, indicates that, as the carbonate concentration in solution is maximized, the calcium concentration remaining in solution should be minimized. However, softening efficiencies for the first three series, where aragonite was the predominant crystal form, did not vary significantly at the $\alpha = 0.05$ significance level. The softening efficiency was actually 0.1% higher for Series III than for Series I, where the carbonate concentration was greatest. This implies that factors other than the solubility product relationship between calcium and carbonate concentrations are involved in the degree of hardness removal in systems where aragonite calcium carbonate crystals are formed.

As with the crystal habit and kinetic data, the effluent hardness levels were substantially lower in Series IV than in the other three series. Series IV, where calcite crystals predominated, softening efficiencies averaged 90% versus 74-78% for the three series where most crystals were aragonite. Intuitively, one would conclude that either the softening efficiencies or the effluent

Table 6. Hardness data for individual runs

Run-Series	Initial hardness, ppm as $CaCO_3$	Effluent hardness, ppm as $CaCO_3$	Softening efficiency, %	Ionic strength, mole/l x 10^3	K_{sp}' x 10^9	$[(Ca^{++}][CO_3^{=}]$ - K_{sp}') x 10^7
7-I	232.2	57.0	75.4	3.35	9.31	2.82
8	245.6	48.2	80.4	3.32	9.29	1.30
9	230.1	44.7	80.6	3.18	9.23	1.91
11	230.5	55.5	75.9	3.26	9.27	2.02
16-II	224.4	61.7	72.5	3.42	9.33	2.81
17	225.4	56.2	75.1	3.18	9.23	2.14
19	222.9	58.4	73.8	3.39	9.33	2.53
21	220.9	57.4	74.0	3.33	9.29	1.88
22	219.6	50.7	76.9	3.23	9.25	1.59
20-III	238.0	58.0	75.6	4.11	9.66	1.53
23	238.0	51.8	78.2	4.68	9.90	1.74
25	232.8	40.8	82.5	4.63	9.88	0.938
26	233.9	54.8	76.5	5.42	10.2	1.31
29-IV	365.4	33.8	90.7	4.67	7.34	0.680
30	361.7	43.8	87.9	4.64	7.33	1.00
31	352.4	33.1	90.6	4.74	7.36	1.07
32	367.1	36.9	89.9	4.80	7.38	1.02

Table 7. Series averages for hardness data

Series	Initial hardness, ppm as $CaCO_3$	Final hardness, ppm as $CaCO_3$	Softening efficiency, %	Ionic strength, mole/l x 10^3	K_{sp}' x 10^9	$[(Ca^{++}][CO_3^{=}]$ - K_{sp}') x 10^7
I	234.6	51.4	78.1	3.28	9.28	2.01
II	222.6	56.9	74.4	3.31	9.29	2.19
III	235.7	51.4	78.2	4.71	9.91	1.38
IV	361.6	36.9	89.8	4.71	7.35	0.942

hardness levels would remain constant as the initial hardness is increased. The fact that the effluent hardness is lower for the high initial hardness implies the hardness removal is dependent in some way on the initial hardness or the difference between initial and effluent hardness levels. This phenomenon is not understood at this time. Stumm and Morgan (42) noted the solubility of aragonite is roughly one ppm higher than that of calcite. It is not felt this difference is sufficient to explain the difference in effluent hardness levels between the calcite-forming runs in Series IV and the aragonite-forming runs in Series I-III.

The equilibrium solubility of calcium carbonate in an ideal solution is 7-8 ppm. At the ionic strengths encountered in this research, the maximum corrected solubility was 10.1 ppm. The corrected solubility product was calculated from Equation (E 7):

$$pK_{sp}' = pK_{sp} - 4\sqrt{I}/(1 + 3.9\sqrt{I}) \qquad \text{(E 7)}$$

where pK_{sp} = -8.22 for aragonite and -8.35 for calcite (42). These equilibrium conditions were not reached. Table 7 shows the effluent levels in the first three series clustered around 47 ppm, while those in Series IV averaged 37 ppm. These values suggest that a plateau, or "pseudo-equilibrium," was reached below which no additional hardness was removed in the residence times studied. The softening efficiencies do not consistently change as the residence time increases, indicating this pseudo-equilibrium is reached in less than 20 minutes. The fact that the softening efficiencies

do not change as residence time increases also implies the residence time could possibly be decreased below 20 minutes without decreasing softening efficiency for a given set of initial conditions.

Alkalinity Results

The alkalinity distribution was very important in this research as it determined the amount of carbonate available for precipitation. The ratio of total to phenolphthalein alkalinities (T/P) was used as a controlling parameter in this research.

Tables 8 and 9 list alkalinity and pH data for individual runs and series averages, respectively. A Beckman pH meter was used in Runs 7, 9, and 16. Table 8 shows the effluent pH in these runs was substantially lower than in the other runs of Series I and II. The Beckman meter data was judged less accurate than the more precise Corning pH meter used in all other runs.

Schierholz (37) studied the equilibrium relations in calcium carbonate precipitation to show the carbonate alkalinity is a maximum at T/P = 2.0. Table 9 indicates the carbonate alkalinity is indeed a maximum at T/P = 2.0 in this research, agreeing with the derivation of Schierholz.

As with the other measurements, Series IV differed from the other three series. For Series I through III, the carbonate alkalinity decreases as the hydroxyl alkalinity increases. Series IV was conducted at a hydroxyl alkalinity between those of Series

Table 8. Alkalinity measurements for individual runs

Run	Series	τ, min	Effluent pH	Alkalinities, mg/l				
				T	P	OH	CO_3	HCO_3
7		29.9	9.955[a]	60.0	30.1	4.5	51.2	4.3
8	I	20.3	10.251	43.7	23.4	8.9	29.0	5.8
9		39.8	9.84[a]	50.9	25.9	3.5	44.8	2.6
11	-	29.8	10.411	59.3	31.9	12.9	38.0	8.4
16		29.8	9.674[a]	57.0	25.9	2.4	47.0	7.6
17		19.8	9.895	54.6	23.8	3.9	39.8	10.9
19	II	39.3	10.301	71.1	32.5	10.0	45.0	16.1
21		29.4	10.298	60.9	27.1	9.9	34.4	16.6
22	-	19.9	10.166	58.3	23.9	7.3	33.2	17.8
20		29.4	10.856	72.7	49.9	35.9	28.0	8.8
23	III	38.5	11.011	96.1	69.1	51.3	35.6	9.2
25		19.7	11.009	85.0	63.7	51.0	25.4	8.6
26	-	18.9	11.118	113.9	88.6	75.7	25.8	12.4
29		19.5	10.533	48.1	28.3	17.1	22.3	8.7
30	IV	29.4	10.620	50.6	33.3	21.0	24.6	5.0
31		38.1	10.635	63.7	39.0	21.6	34.7	7.3
32		29.4	10.655	59.2	37.5	22.6	29.8	6.9

[a]Beckman pH meter.

Table 9. Series averages for alkalinity data

Series	Effluent pH	T/P ratio	Alkalinities, mg/l				
			T	P	OH	CO_3	HCO_3
I	10.114	1.92	53.5	27.8	7.4	40.8	5.3
II	10.067	2.27	60.4	26.6	6.7	39.9	13.8
III	10.998	1.36	91.9	67.8	53.5	28.7	9.8
IV	10.611	1.60	55.4	34.5	20.6	27.9	7.0

I and III, but the carbonate alkalinity was actually lower than that of Series III. This lowered alkalinity appears related to the increased softening efficiencies in the fourth series.

In Series III, the CSD shifted in the 20- and 30-minute residence time runs, while the shift generally did not occur in Series I and II. Since the residual hardness levels were roughly equal in the three series, the decrease in carbonate concentration in Series III appears sufficient to initiate the aragonite to calcite shift.

Kinetic Order Correlations

Schierholz (37) noted that the carbonate alkalinity was lower for higher kinetic orders. A goal of this research was to determine if a similar trend developed in an unscraped continuous reactor. Figure 25 is a plot of kinetic order vs carbonate alkalinity for the four series of runs. The slope of the line is -0.288, and the intercept was 13.6. The correlation coefficient was -0.997.

Series IV was performed to determine if the kinetic order-carbonate plot could predict behavior of a set of runs with a higher initial hardness at an intermediate lime treatment. At the time, it was assumed Series IV runs would produce aragonite crystals during kinetic measurements. The three points representing the 225 ppm initial hardness series predict a kinetic order of three to four at approximately 35 mg/l carbonate alkalinity at T/P = 1.6. While the kinetic order and carbonate alkalinity differed from

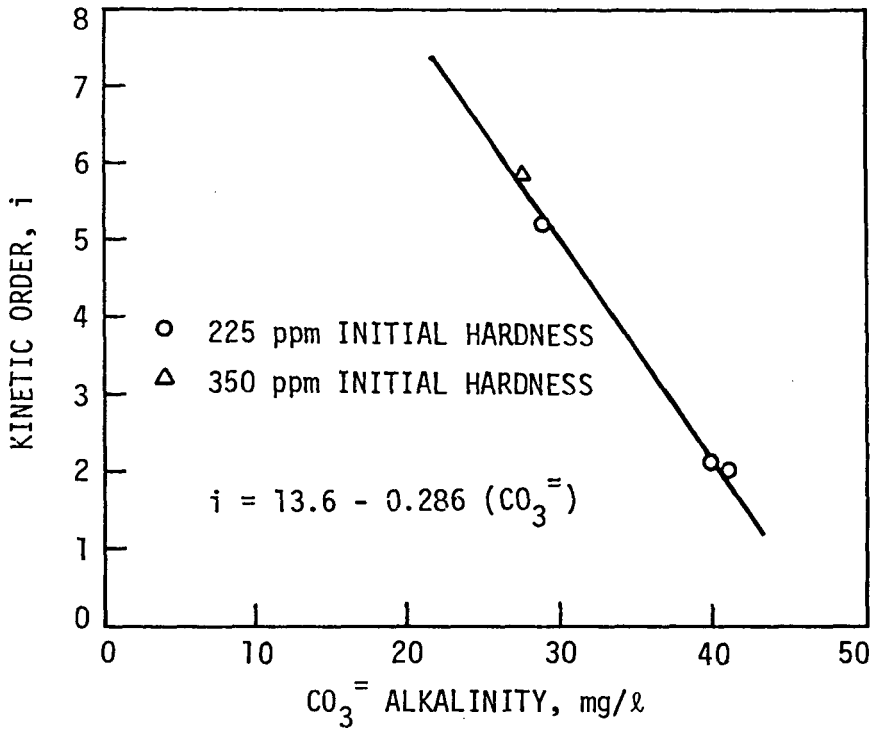

Figure 25. Kinetic order, i, vs carbonate ion concentration

the predicted values, Figure 25 is extremely interesting in that the Series IV point (denoted in Figure 25 by an "X" in the circle) remained on the kinetic order-carbonate line in spite of the many differences between Series IV and the other runs.

Stevens et al. (41) observed a linear correlation between kinetic order and hydroxyl alkalinity in a system precipitating magnesium hydroxide. It seems reasonable that kinetic order-carbonate alkalinity data from a series of runs performed at a T/P ratio of 1.6-1.7 and 225 ppm initial hardness would lie close to the line plotted in Figure 25, since three other series lie along the line. Extrapolation of this line beyond the range of 27-41 mg/l carbonate alkalinity without experimental data is not recommended, as kinetic behavior in these regions is unknown. A series performed at T/P = 1.6-1.7 would therefore yield much information of the predictive value of Figure 25 at 225 ppm initial calcium levels.

Though the Series IV point also lies along the line in Figure 25, it is unknown if this figure predicts kinetic order-carbonate alkalinity as a function of initial hardness since kinetic measurements in this series were taken while the predominate crystal habit was calcite instead of the aragonite habit measured in Series I-III. While the 350-360 initial hardness system may indeed produce data lying along this line, the fact that calcite is formed instead of aragonite may cause the kinetic order-carbonate line slope to increase or decrease. Two series, performed at 350-360 ppm initial

hardness and T/P ratios of 2.0 and 1.4, are necessary to determine kinetic order-carbonate data when calcite crystals are produced.

Reddy and Nancollas (34) found growth rate on a seed crystal was a linear function of residual supersaturation (defined as the product of calcium and carbonate concentrations minus a corrected solubility product). Figure 26 is a plot of kinetic order versus residual supersaturation. As with Figure 25, Figure 26 exhibits a negative slope. There is considerably more deviation from the least-squares fit in the kinetic order-residual supersaturation plot than in Figure 25 for the three series where aragonite kinetic measurements were made, implying Figure 26 is less valuable for predictions at other T/P conditions at 225 ppm initial hardness conditions. Predictions of kinetic order-residual supersaturation data as a function of initial hardness using Series IV (denoted as a triangle in Figure 26) should be avoided for the same reasons given for Figure 25.

In summary, information gained from Figures 25 and 26 is among the most important gathered in this research. Even though the kinetic order does not remain constant from run to run as in the case in concentrated crystallization systems, these plots are the first known attempt to correlate the kinetic orders found in continuous calcium carbonate precipitation with driving forces present in the reaction system. Figures 25 and 26 do not contain all information necessary to quantitatively predict the kinetic order at a given initial hardness and T/P ratio, but they do indicate that

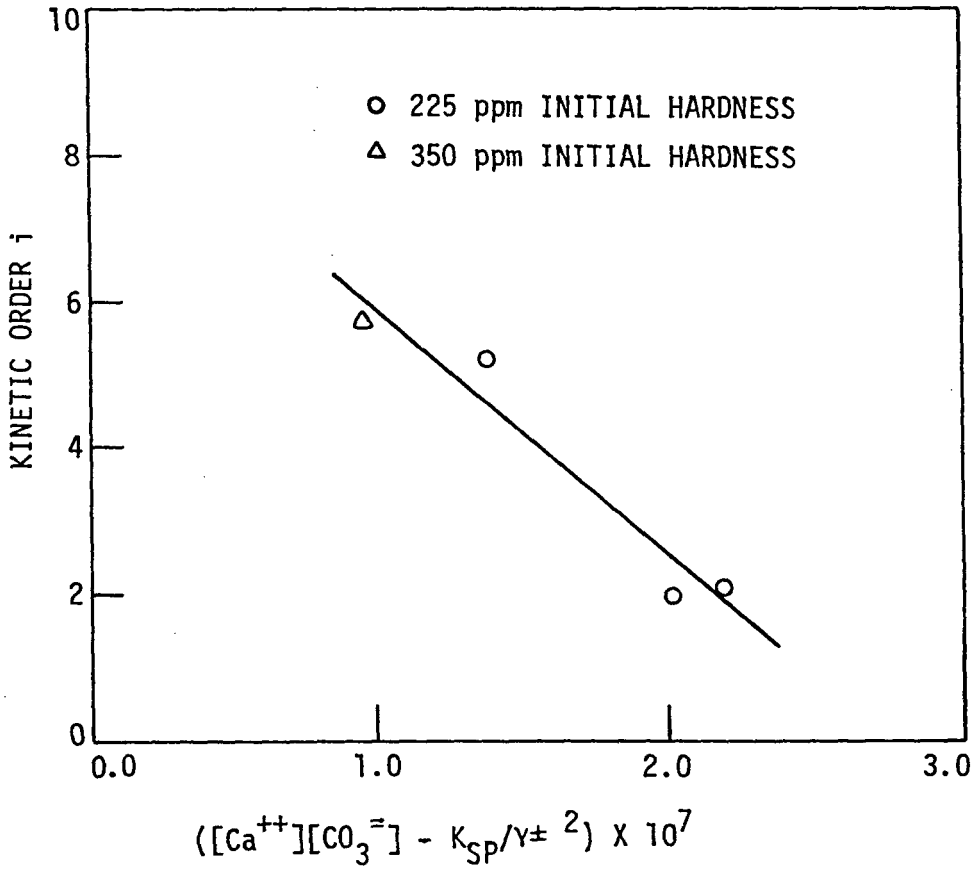

Fig. 26. Kinetic order vs. supersaturation data

definite trends exist. These trends point to other reactor conditions which, when kinetic data are obtained at these conditions, would allow a priori kinetic order predictions.

Equilibrium Studies

Samples were collected at 15-16 residence times in several runs to determine to what hardness and pH the reactor effluent equilibrates. Both filtered and unfiltered reactor effluent samples were collected.

A sampling procedure which minimizing CO_2 absorption and pH variations was not developed until late in the research. In addition, the samples appeared to be stable only for about a week. After this time, hardness and pH values fluctuated by at least 10 ppm calcium and at least 0.4 pH units, respectively. Therefore, only a very few samples yielded reasonably consistent equilibrium data.

Samples from Run 32 supplied the most uniform equilibrium measurements. Figures 27 and 28 depict this data for filtered and unfiltered samples. As Figure 27 shows, the residual hardness changed by 14% for the four filtered samples and 12% for the first three unfiltered effluent samples. The final unfiltered hardness sample was 2-3 ppm lower than the other samples, probably because it was the only sample taken from a previously opened flask. The samples filtered during removal from the reactor had more constant pH values than the unfiltered samples, as shown in Figure 28. This

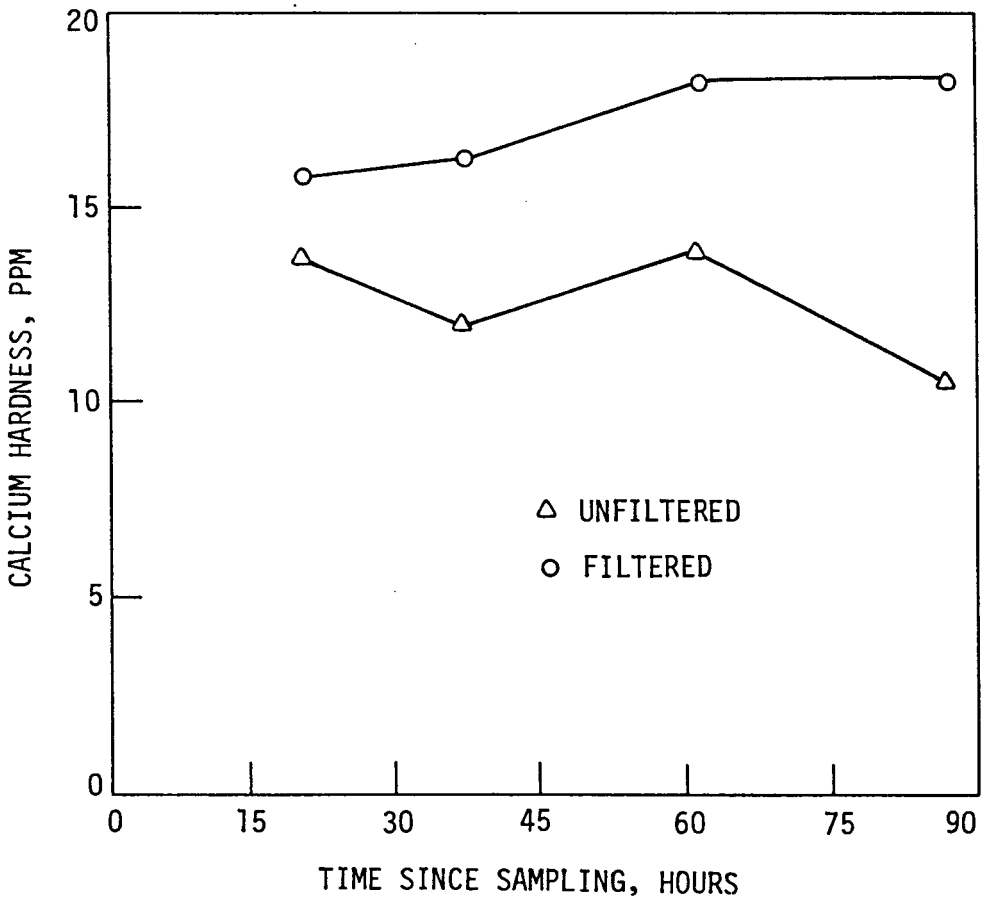

Fig. 27. Residual calcium hardness vs time equilibrium data for run 32

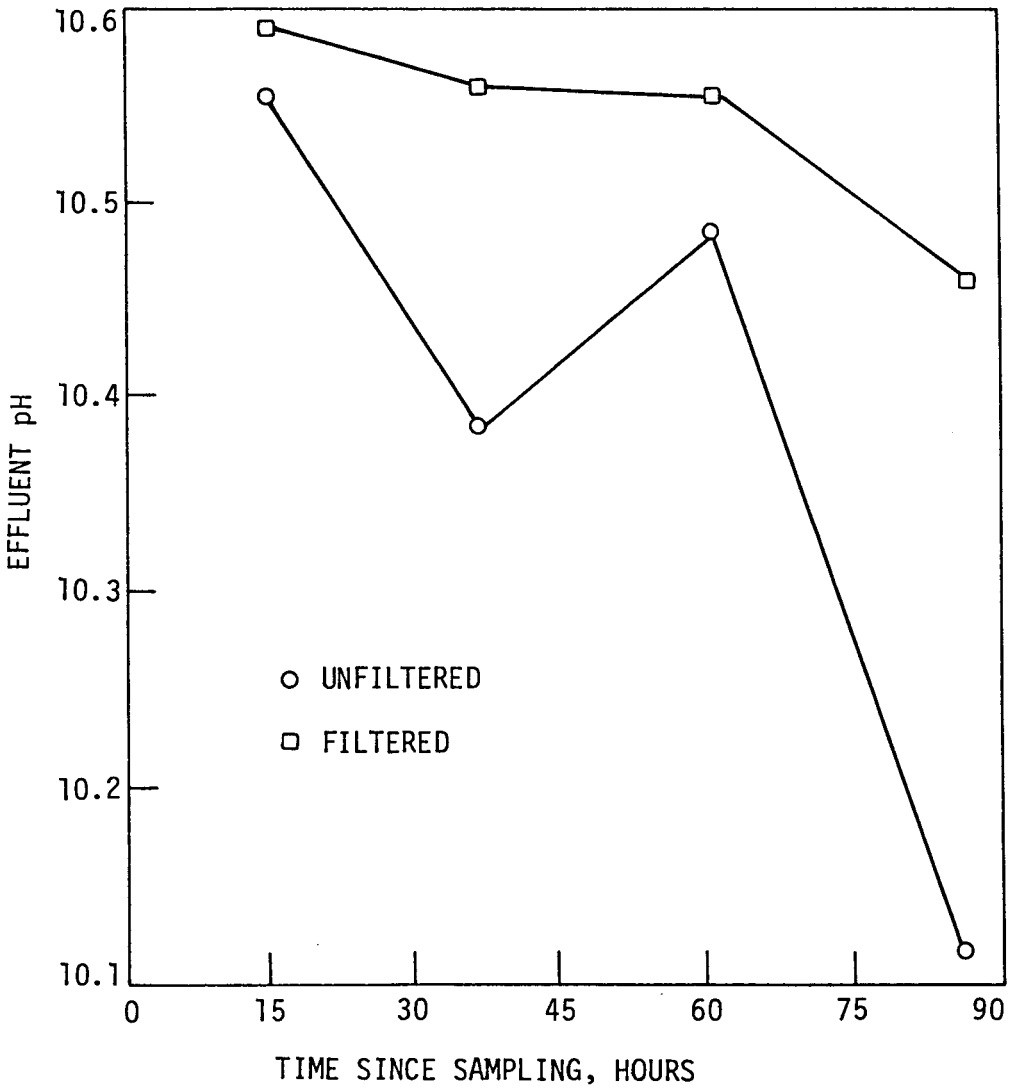

Fig. 28. pH vs. time data for run 32 equilibrium samples

indicates the crystals in solution reduce stability, presumably due to CO_2 absorption.

A major problem with equilibrium sampling is implied from the crystal morphology section. In some runs, the predominant crystal form is aragonite, while in other runs the habit is calcite. In addition, aragonite crystals left in solution for several hours appear to rearrange to the calcite form. The equilibrium solubility of aragonite is slightly higher than that of calcite (42). These questions arise: Which calcium carbonate crystal form is present in the equilibrium samples at the time of analysis? Is this the same form which existed in the reactor during sampling? If not, the equilibria determined from the equilibrium sampling are not those present during the experimental run. Further studies of equilibrium reactor conditions and crystal structure must be conducted before these questions can be satisfactorily answered.

Suspension Density and Mass Balances

Table 10 lists suspension densities, total reactor wall depositions, and mass balance closure percentages. The suspension densities were determined by direct measurements and by a calcium mass balance. Since the two suspension density values for each run do not agree with each other, the suspension densities taken from direct measurement (M_{T_1}) were used to ascertain calcium and carbonate-bicarbonate mass balance closure percentages.

Table 10 shows that the suspension densities for Series IV

Table 10. Suspension density and mass balance data

Run	Series	τ, min	M_{T_1},[a] g/l	M_{T_2},[a] g/l	Total deposition, g	Suspension weight / Deposition weight	Calcium closure, %	Carbonate-bicarbonate closure, %
7		29.9	0.0810	0.1121	17.79	1.34	86.2	90.4
8	I	20.3	0.1031	0.1594	10.96	2.80	88.5	90.1
9		39.8	0.0942	0.1032	24.21	1.17	96.2	103.2
11	—	29.8	0.1025	0.1093	20.66	1.60	96.6	101.6
16		29.8	0.0821	0.0977	18.75	1.30	92.9	92.2
17		19.8	0.0752	0.1221	13.68	1.69	78.9	81.3
19	II	39.3	0.0512	0.0752	24.57	0.59	89.2	96.4
21		29.4	0.0823	0.1032	17.58	1.43	90.7	93.1
22	—	19.9	0.0630	0.1287	13.12	1.60	72.9	82.1
20		29.4	0.1244	0.1229	16.55	2.36	102.1	104.0
23	III	38.5	0.1305	0.1178	17.76	2.16	107.1	114.6
25		19.7	0.1026	0.1424	14.28	2.28	82.6	85.1
26	—	18.9	0.0983	0.1204	14.48	2.12	90.0	90.9
29		19.5	0.2256	0.2534	21.54	3.15	92.1	98.9
30	IV	29.4	0.2297	0.2094	30.34	2.26	104.1	107.3
31		38.1	0.2087	0.1664	39.98	1.49	112.2	129.2
32		29.4	0.2032	0.2120	32.08	1.94	99.3	105.7

[a]Suspension density determined by: 1. direct measurement; 2. calcium mass balance.

are roughly twice those of Series III, and that the M_{T_1} values increase gradually with increasing lime dosage for the first three series. Series IV runs have larger suspension densities because nearly twice as many ppm calcium hardness was removed in the runs than in the first three series.

Series III may have higher suspension densities than Series I and II because of the shifting from larger aragonite crystals to smaller calcite crystals in three Series III runs. Dendritic aragonite crystals, due to the protruding "needles," are more likely to become intertwined with each other than calcite crystals; hence, fewer calcite crystals stick to crystals previously adhered to the reactor surfaces. The higher suspension weight/deposition weight ratios found in both Series III and IV, where calcite was the major crystal form at the end of the runs, support this hypothesis.

CONCLUSIONS

1. The crystal habit varies as a function of supersaturation. Dendritic aragonite crystals form at high residual supersaturations, and rhombic calcite crystals develop residual supersaturations. A critical residual supersaturation exists separating the crystal habits.

2. The crystal size distribution shifts toward the lower sizes in several runs. The shift is due to crystals changing from aragonite to calcite as the residual supersaturation decreases during the run.

3. A power law kinetic model can be used to describe calcium carbonate precipitation kinetics. The power law expressions for systems with 225 ppm initial hardness are:

$$B^o = 8.0 \times 10^2 \, G^{2.1} \text{ at } T/P = 2.25$$

$$B^o = 1.6 \times 10^3 \, G^{2.0} \text{ at } T/P = 2.0$$

$$B^o = 1.1 \times 10^5 \, G^{5.2} \text{ at } T/P = 1.4$$

At 350 ppm initial hardness, the expression was

$$B^o = 7.3 \times 10^6 \, G^{5.8} \text{ at } T/P = 1.6$$

4. Aragonite is the major crystal form for 225 ppm initial hardness experiments, while calcite predominates at 350 ppm initial hardness. Comparisons between data obtained with different crystal habits are thus complicated.

5. Softening efficiencies average 90% for runs where calcite predominate and 74-78% where aragonite is the major crystal habit.

6. Kinetic orders correlate linearly with carbonate alkalinity and residual supersaturation. However, it is unclear at this time whether these correlations can be used for a priori predictions of kinetic order at untested initial conditions.

7. A procedure was developed to study equilibrium reactor effluent conditions for as long as a week after a run. However, it is not known if the equilibria studied are the same as those found during the run due to possible changes in crystal habit.

8. A large percentage of crystals produced during the runs adhere to reactor surfaces instead of remaining in suspension. A smaller percentage of calcite adhere than aragonite, due to the dendritic nature of aragonite.

RECOMMENDATIONS

1. A series of runs at 225 ppm initial calcium hardness and T/P ratio of 1.6-1.7 should be conducted using the same reactor and experimental procedure to determine the predictive value of the kinetic order-carbonate plot at intermediate T/P conditions and to further define the critical residual supersaturation between aragonite and calcite crystal habits by determining the effect of residence time length on the ratio of aragonite to calcite crystals.

2. The effects of initial hardness level on crystallization kinetics and the aragonite/calcite crystal habit ratio should be examined.

3. Calcium carbonate crystallization kinetics should be studied using a recycle stream to return larger crystals to the reactor. Initial calcium levels for this study should be sufficiently high to produce large numbers of mostly calcite crystals to reduce wall scale and allow for the return of many crystals to the reactor, thus increasing the reactor suspension density.

4. The precipitation of a sparingly soluble salt not found in the water softening process should be studied to see if the kinetic order changing with initial conditions is characteristic of all continuous precipitation systems or just the water softening system. One such salt could be zinc carbonate ($K_{sp} = 3 \times 10^{-8}$).

5. The addition of various dosages of a polyelectrolyte to initial conditions studied in this research should be investigated

to determine flocculation and agglomeration effects on the precipitation kinetics.

BIBLIOGRAPHY

1. Abegg, C. F., J. D. Stevens, and M. A. Larson. 1968. Crystal size distributions in continuous crystallizers when growth is size dependent. A.I.Ch.E. J. 14:118-122.

2. Adamson, A. W. 1973. A textbook of physical chemistry. Academic Press, New York, New York. 1073 pp.

3. Alexander, H. J., and M. A. McClanahan. 1975. Kinetics of calcium carbonate precipitation in lime-soda ash softening. J. Am. Water Works Assoc. 67:618-621.

4. Behrman, A. S., and W. H. Green. 1939. Accelerated lime-soda water softening. Ind. Eng. Chem. 31:128-133.

5. Clark, J. W., W. Viessman, Jr., and M. J. Hammer. 1977. Water supply and pollution control. 3rd ed. International Textbook Co., Scranton, Pa. 831 pp.

6. Cleasby, J. L. 1958. Report of increased capacity studies of the present municipal water treatment plant in Ames, Iowa. Ames, Iowa, Dept. of Civil Engrg., Iowa State University.

7. Coulter Electronics, Inc. 1975. Operator's manual for the coulter counter model TA II. Author, Hialeah, Fla.

8. Dabir, B. 1978. On the precipitation of $Mg(OH)_2$ in water softening. M.S. Thesis. Iowa State University, Ames, Iowa.

9. Dallons, V. J. 1972. Point source secondary nucleation studies in a MSMPR crystallizer. M.S. Thesis. Iowa State University, Ames, Iowa.

10. Dedek, J. 1966. Le carbonate de chaux. Louvain, Librairie Universitaire. 351 pp.

11. Diehl, H. C. 1970. Quantitative analysis. Oakland Street Science Press, Ames, Iowa. 454 pp.

12. Dye, J. F. 1952. Calculation of effect of temperature on pH, free carbon dioxide, and the three forms of alkalinity. J. Am. Water Works Assoc. 44:356-372.

13. Dye, J. F., and J. L. Tuepker. 1971. Chemistry of the lime-soda process. American Water Works Association. 3rd ed. McGraw-Hill, New York, N.Y.

14. Fair, G. M., J. C. Geyer, and D. A. Okun. 1968. Water and wastewater engineering. John Wiley and Sons, Inc., New York, N.Y.

15. Feitler, H. 1972. Cooling water scale control: The scale meter and the critical pH of scaling. Materials Protection and Performance 11:29-33.

16. Garrels, R., and C. Christ. 1965. Solutions, minerals, and equilibria. Harper and Row, New York, N.Y. 435 pp.

17. Harned, H. S., and B. B. Owen. 1950. The physical chemistry of electrolytic solutions. Reinhold Publishing Co., New York, N.Y.

18. Harned, H. S., and S. R. Scholes, Jr. 1941. The ionization constant of HCO_3^- from 0^o to 50^o. J. Amer. Chem. Soc. 63: 1706-1709.

19. Juzaszek, P. and M. A. Larson. 1977. Influence of lines dissolving on crystal size distribution in an MSMPR crystallizer. A.I.Ch.E. J. 23:460-468.

20. Kemmer, F. N., Tech. Ed. 1977. Water: The universal solvent. Nalco Chemical, Oak Brook, Ill. 155 pp.

21. Langelier, W. F. 1936. The analytical control of anticorrosion water treatment. J. Am. Water Works Assoc. 28:1500-1521.

22. Larson, M. A. 1978. Guidelines for selecting a crystallizer. Chem. Eng. 85:90-102.

23. Larson, T. E., and A. M. Buswell. 1942. Calcium carbonate saturation index and alkalinity interpretations. J. Am. Water Works Assoc. 34:1667-1684.

24. Larson, T. E., R. W. Lane, and C. H. Neff. 1959. Stabilization of magnesium hydroxide in the solids contact process. J. Am. Water Works Assoc. 51:1551-1558.

25. Larson, T. E., F. W. Sollo, Jr., and F. F. McGurk. 1976. Complexes affecting the solubility of calcium carbonate in water--phase II. Illinois University Water Resources Center Research Report No. 108.

26. Maruscak, A., C. G. Baker, and M. A. Bergoughou. 1971. Calcium carbonate precipitation in a continuous stirred tank reactor. Can. J. Chem. Eng. 49:819-827.

27. Mullin, J. W. 1972. Crystallisation. Butterworths, London. 480 pp.

28. Nancollas, G. H., and M. M. Reddy. 1971. The crystallization of calcium carbonate. II. Calcite growth mechanism. J. Colloid Interface Sci. 37:824-830.

29. Nauman, E. B. 1971. Selective fines destruction in recycle crystallizers. A.I.Ch.E. Sym. Series 110, 67:116-120.

30. Nauman, E. B., and T. T. Szabo. 1971. Nonselective fines destruction in recycle crystallizers. A.I.Ch.E. Sym. Series 110, 67:108-115.

31. Peters, R. W. 1978. The co-precipitation of calcium carbonate and magnesium hydroxide in an unseeded system. M.S. Thesis. Iowa State University, Ames, Iowa.

32. Randolph, A. D. 1970. How to approach the problems of crystallization. Chem. Eng. 77:80-96.

33. Randolph, A. D., and M. A. Larson. 1971. Theory of particulate processes. Academic Press, New York, N.Y. 251 pp.

34. Reddy, M. M., and G. H. Nancollas. 1971. The crystallization of calcium carbonate. I. Isotopic exchange and kinetics. J. Colloid Interface Sci. 36:166-172.

35. Ryznar, J. W. 1944. A new index for determining amount of calcium carbonate scale formed by a water. J. Am. Water Works Assoc. 36:472-486.

36. Sawyer, C. N. and P. L. McCarty. 1967. Chemistry for sanitary engineers. McGraw-Hill, New York, N.Y.

37. Schierholz, P. M. 1974. Kinetics of crystallization in a dilute system. Ph.D. Thesis. Iowa State University, Ames, Iowa.

38. Shreve, R. N. 1967. Chemical process industries. 3rd ed. McGraw-Hill, New York, N.Y. 905 pp.

39. Sidkar, S. K., and A. D. Randolph. 1976. Secondary nucleation of two fast growth systems in a mixed suspension crystallizer: Magnesium sulfate and citric acid water systems. A.I.Ch.E. J. 22:110-117.

40. Standard Methods for the Examination of Water and Wastewater. American Public Health Association, Inc., New York, N.Y. 769 pp.

41. Stevens, J. D., B. Dabir, and R. W. Peters. 1979. Crystal nucleation and growth in the water softening process. B. F. Ruth Symposium Proceedings, Iowa State University, Ames, Iowa.

42. Stumm, W., and J. J. Morgan. 1970. Aquatic Chemistry. Wiley-Interscience, New York, N.Y. 583 pp.

43. Wiechers, H. N. S., P. Sturrock, and G. V. R. Marias. 1975. Calcium carbonate crystallization kinetics. Water Res. 9:835-845.

44. Wray, J. L., and F. Daniels. 1957. Precipitation of calcite and aragonite. J. Amer. Chem. Soc. 79:2031-2034.

ACKNOWLEDGEMENTS

I wish to thank Dr. J. D. Stevens for his guidance and constructive suggestions offered throughout this research. This guidance is deeply appreciated. I also thank Drs. M. A. Larson and C. S. Oulman for serving on my committee. Discussions with fellow graduate student Bob Peters concerning experimental procedures and results are also highly valued.

I am grateful to Mark Ingebretson and Steve Mueller for their assistance in performing the experiments. Jerry Amenson took the scanning electron microscope photomicrographs, and Mrs. Anita Serovy typed the manuscript. These people are also appreciated.

I also thank the Department of Chemical Engineering, the National Science Foundation, and the Engineering Research Institute for financial support.

Finally, I wish to say a big "thank you" to a special friend, Jane Lowry, who provided much encouragement throughout the latter part of this project, and to my parents, who have loved me and encouraged me immeasurably throughout my stay at Iowa State University.

APPENDIX

An initial objective of this project was to determine calcium carbonate precipitation kinetics in a seeded system in which a recycle stream was utilized to return only larger crystals to the reactor. The kinetics of the seeded system were to be compared with the kinetics of the unseeded system at conditions of maximum carbonate alkalinity (Series I) and with the results of Schierholz. Three runs were performed at 225 ppm initial hardness and T/P ratio of 2.0 using a 4000-ml separatory funnel to separate the reactor effluent into fractions of predominantly larger and smaller crystals. Another gravity-separation device was designed to provide better separation, but the seeded experiments were discontinued before the new separator was tested when the need for improved unseeded kinetic measurements became apparent.

Background

In many municipal softening plants, precipitated sludge collected at the bottom of the settling tank is recycled to the reactor. This sludge contains mostly larger crystals, as the smallest crystals do not settle out in the settling tank. Softening reactors employing recycle streams can be approximated by fines-dissolving crystallizers using the Randolph-Larson MSMPR model with the relaxation of the assumption that no crystals are present in the feed streams. Figure 29 illustrates hypothetical fines-dissolving operation on a cumulative numbers-crystal length plot. The solid line depicts

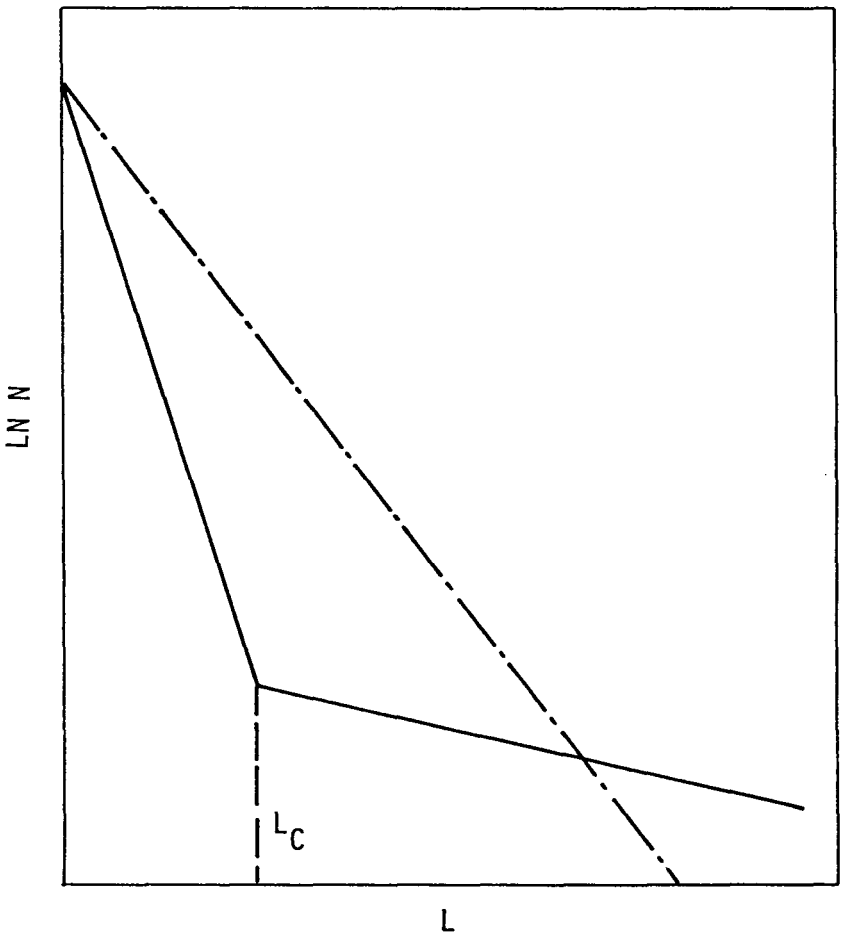

Fig. 29. Effect of fines dissolving

fines-dissolving, while the dotted line represents MSMPR operation. A much higher percentage of crystals above a cut size L_c exists in fines-dissolving than in MSMPR crystallizers. Recycle of predominantly larger crystals is necessary because Nauman (29) and Nauman and Szabo (30) showed that, if fines dissolving is employed, the dominant size is increased, but the dominant size is actually decreased when particles of all sizes are returned to the reactor.

Experimental

Experimental equipment consisted of all equipment used in the unseeded runs plus these major additions:

(1) A 4000-ml separatory funnel

(2) A two-sided Gorman-Rupp Industries Model bellows pump

(3) A Masterflex Model WZ1RO31 variable speed pump and controller with a 7015 pump head.

One side of the bellows pump transported part of the reactor effluent to the separatory funnel. The reactor withdrawal tube was a stainless steel tube with a 90^{o} polyethylene elbow placed in the reactor so that the tube entrance was 10-12 centimeters below the 16-liter level and perpendicular to the suspension flow. The Masterflex pumped the separatory funnel supernatant from the funnel to the drain. The funnel slurry flowed through the funnel stopcock to a 1000-ml flask. This flask was kept approximately half full with slurry and was slowly stirred magnetically to prevent settling. The slurry was pumped to the reactor with the other side of the

bellows pump. The two-sided bellows pump was used to minimize crystal breakage during recycling.

The addition of the separatory funnel and accompanying equipment greatly complicated the experimental procedure. The funnel inlet and outlet flow rates were qualitatively controlled by setting the bellows pump at a constant value and adjusting the supernatant flow rate and funnel stopcock to prevent overflowing and drainage of the funnel. The funnel stopcock required constant attention. This fact, along with the formation of undesired circulation patterns in the funnel which hindered settling, instigated the design of another separatory device. Rotameters which would have improved the control of the funnel inlet and outlet streams did not arrive until after the seeded runs were terminated.

The funnel inlet flow rate in all seeded runs was 200 milliliters per minute, the recycle flow rate was 50 ml/min, and the supernatant flow rate was 150 ml/min. Coulter Counter analyses were performed on the reactor suspension (as described in the body of this thesis), funnel supernatant, and recycle streams. The recycle stream samples were taken by pipetting an aliquot from the 1-liter flask below the funnel and diluting with filtered reactor effluent. The supernatant CSD samples were taken by pumping the supernatant into a 150-ml beaker, pipetting an aliquot from the beaker, and diluting with reactor effluent.

New Separatory Tube

The new gravity separation tube is diagrammed in Figure 30. This glass tube is 8.5 centimeters in diameter and 60 centimeters long, with a conical bottom leading to a 1.5-cm diameter slurry exit port. The inlet is 20 centimeters from the base of the cylindrical tube and is curved upward inside the tube. Preliminary studies using a smaller but similar tube indicated the conical bottom and curved inlet tube were necessary to prevent excessive crystal buildup in the tube base and undesirable flow paterns at the inlet. The separation tube supernatant is removed using a tube placed near the liquid-air interface at the top of the separation tube. A rubber stopper with holes for air and this withdrawal tube is inserted into the top of the separation tube.

Crystal settling velocities were determined by (5):

$$u_+ = \frac{gD_p^2 (\rho_p - \rho)}{18\mu} \qquad \text{(E48)}$$

This equation is valid because the particle Reynolds number is less than 0.3. Equation (E48) also assumes spherical particles. Photomicrographs presented earlier show this assumption is not valid for either calcite or aragonite; however, the fact that calcite crystals have much less void space than aragonite implies that the initial reactor hardness should be high enough to form calcite crystals to minimize the invalidity of this assumption.

The separation tube was designed to provide a cut size L_c of

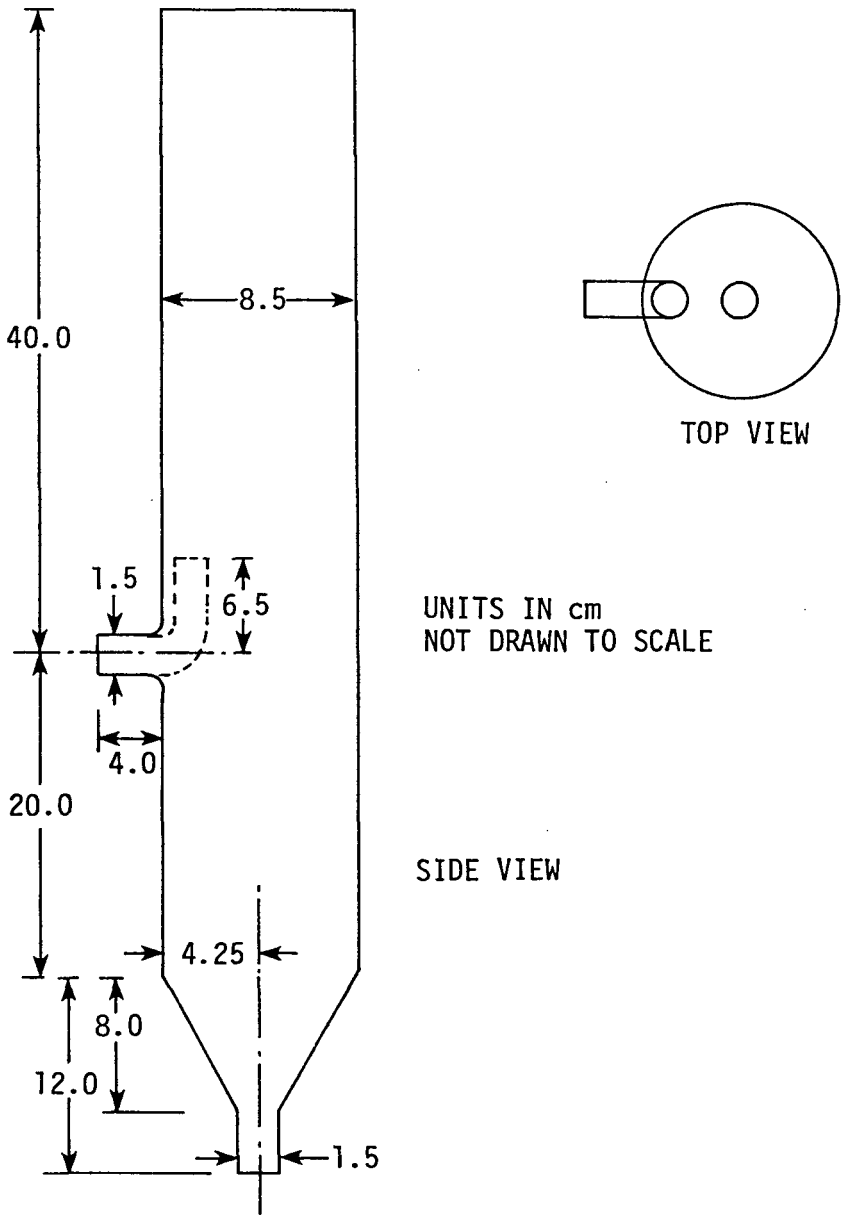

Fig. 30. Gravity separation tube

20 microns at a tube inlet flow rate of 250 milliliters per minute and a recycle stream flow rate of 125 ml/min. These flow rates were set so that the settling velocity of 20-micron crystals according to Equation (E48), 0.0409 cm/sec, was slightly greater than the upward velocity of water leaving the tube in the supernatant stream (0.0367 cm/sec). The water velocity was calculated by dividing the supernatant flow rate by the tube cross-sectional area. This 0.004 cm/second velocity difference should be sufficient to overcome reductions in particle settling velocity due to crystal habit. If not, the cut size can be increased by reducing the flow rate of the supernatant stream.

While the tube is as yet untested, it should produce a better separation than the separatory funnel for several reasons. First, the cut size can be more easily varied in the separation tube. Second, the conical shape of the separatory funnel caused many of the larger crystals to adhere to the funnel walls and created many flow patterns detrimental to particle settling. The cylindrical shape of the tube should reduce both these effects. Third, the inlet tube is located far enough from the top of the tube so that a quiescent zone, ideal for settling, is created well below the top of the tube. Fourth, the increased volume of the tube should also reduce formation and extent of flow patterns.

Discussion of Separatory Funnel Runs

No reliable crystal size distribution data were obtained in the seeded runs. The seeded system never appeared to reach steady state conditions, as the reactor suspension, supernatant stream, and recycle stream Coulter Counter measurements all varied widely in terms of particle counts and size distribution.

The only reactor suspension CSD samples even resembling fines-dissolving operation were taken in Run 14, the third and final seeded run. Figure 31 displays cumulative numbers-length data for a CSD sample from this run. The figure shows a slight tendency toward fines-dissolving operation, with a cut size of roughly 15 microns. Since the difference between a normal MSMPR cumulative numbers-length plot and Figure 31 is so small, it was concluded a better method of effluent crystal size separation than the separatory funnel is necessary for fines-dissolving operation.

The major problems with separatory funnel usage were the excessive crystal deposition on the conical funnel walls and the constant adjustment of the funnel stopcock necessary to prevent funnel overflow or drainage. Due to the sloping of the funnel walls, nearly all settling crystals would hit and adhere to the funnel walls. This wall deposition was reduced by intermittent opening and closing of the stopcock, but the opening and closing greatly magnified the chance of human error, causing overflowing of the funnel and drainage of the flask below the funnel, thus upsetting steady state conditions in the reactor.

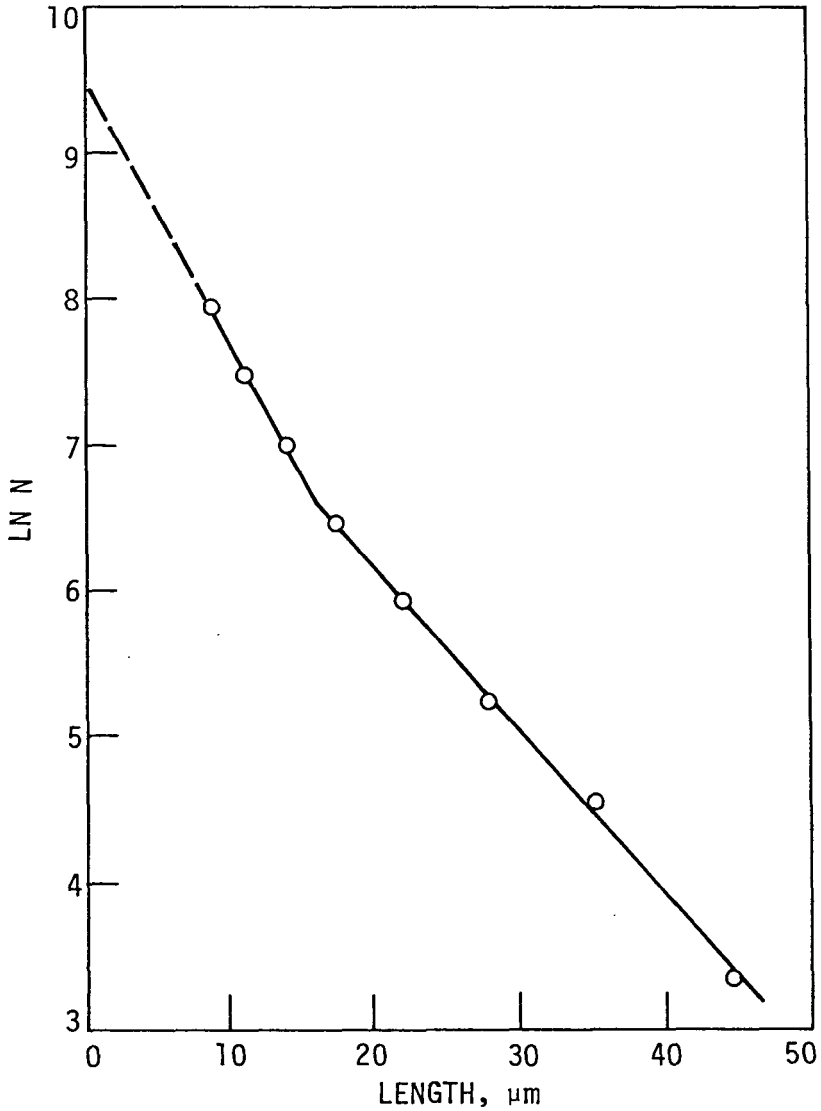

Fig. 31. Ln N vs L plot for seeded run 14

Recommendations

1. The separation tube should be used to produce the separation instead of the separatory funnel.

2. Higher initial hardness levels (350-360 ppm) should be used in the reactor so that calcite crystals are formed. Calcite crystals would:

   (a) be less likely to adhere to reactor and tube walls than aragonite due to their more compact shape;

   (b) have higher settling velocities, also due to their compact shape;

   (c) be formed in greater numbers, because more hardness would be removed and they are smaller than aragonite crystals.

3. Flowmeters should be employed to accurately monitor the inlet and outlet flows of the separation tube.